Hydrogen absorption kinetics at titanium surfaces as measured using ERDA
by Marcus Alton Teter

A thesis submitted in partial fulfillment of the requirements for the degree of Master of Science in Physics
Montana State University

Abstract:
Since titanium alloys are being studied for aerospace usage, the hydrogen absorption characteristics of the alloys must be known. Using titanium metal as a baseline, elastic recoil detection analysis (ERDA) was chosen to measure the hydrogen concentration profile. ERDA allowed for the measurement of both the surface and bulk concentrations of hydrogen with the same experimental equipment, rather than previous methods which required that the two sets of experimental equipment be calibrated with respect to each other. The results allowed for the determination of surface and bulk concentrations of hydrogen as a function of exposure time. ERDA was concluded as being a useful technique for measuring the hydrogen uptake properties of metals.

HYDROGEN ABSORPTION KINETICS AT TITANIUM SUFACES AS MEASURED USING ERDA

By

Marcus Alton Teter

A thesis submitted in partial fulfillment
of the requirements for the degree

of

Master of Science

in

Physics

MONTANA STATE UNIVERSITY, BOZEMAN
Bozeman, Montana

December 1996

APPROVAL

of a thesis submitted by

Marcus Alton Teter

This thesis has been read by each member of the thesis committee and has been found to be satisfactory regarding content, English usage, format, citations, bibliographic style, and consistency, and is ready for submission to the College of Graduate Studies.

Dr. Richard J. Smith — Richard J. Smith (Signature) — 1-27-97 Date

Approved for the Department of Physics

Dr. John C. Hermanson — JHerm (Signature) — 1-27-97 Date

Approved for the College of Graduate Studies

Dr. Robert Brown — RK Brown (Signature) — 2/3/97 Date

STATEMENT OF PERMISSION TO USE

In presenting this thesis in partial fulfillment of the requirements for a master's degree at Montana State University-Bozeman, I agree that the Library shall make it available to borrowers under rules of the Library.

If I have indicated my intention to copyright this thesis by including a copyright notice page, copying is allowable only for scholarly purposes, consistent with "fair use" as prescribed in the U.S. Copyright Law. Requests for permission for extended quotation from or reproduction of this thesis in whole or in parts may be granted only by the copyright holder.

Signature Mary A. Peter

Date 19 DEC 1996

TABLE OF CONTENTS

LIST OF TABLES

LIST OF FIGURES

ABSTRACT

Since titanium alloys are being studied for aerospace usage, the hydrogen absorption characteristics of the alloys must be known. Using titanium metal as a baseline, elastic recoil detection analysis (ERDA) was chosen to measure the hydrogen concentration profile. ERDA allowed for the measurement of both the surface and bulk concentrations of hydrogen with the same experimental equipment, rather than previous methods which required that the two sets of experimental equipment be calibrated with respect to each other. The results allowed for the determination of surface and bulk concentrations of hydrogen as a function of exposure time. ERDA was concluded as being a useful technique for measuring the hydrogen uptake properties of metals.

1.0 INTRODUCTION

Hydrogen absorption by metals has been an ongoing field of investigation for nearly twenty years. Early investigations focused on hydrogen storage techniques, using the metal as a reservoir for the hydrogen. Later, the investigations were geared toward the problem presented by hydrogen embrittlement of materials, especially those materials intended for aerospace applications.

In the case of the national aerospace plane (NASP), the focus has been upon the embrittlement problem. The aerospace plane was intended to be primarily fueled by hydrogen. The weight and strength of materials focused design efforts toward titanium based alloys. Unfortunately, titanium readily absorbs hydrogen, so understanding the characteristics of the absorption and the resulting embrittlement is essential toward using titanium alloys and other materials. In the extreme conditions of flight, there are expected to be thermal conditions which will take materials from cryogenic temperatures to extremely high temperatures in very rapid succession or leave the material at the extremes for long duration. The flight mechanical characteristics for the material must include the ability to withstand high pressure loads and extreme acoustic loads.[1] Any degrading of the titanium alloys by hydrogen would have disastrous effects.

Hydrogen can degrade materials through a number of interactions. On the surface, the hydrogen can be adsorbed to form a hydride. In the bulk, the hydrogen may move into the material forming bonds that lead to hydrides, dislocate substrate atoms that

reduce the material's structural integrity, or form pockets of hydrogen gas.[1] Consequently, material interactions with hydrogen fall into two categories: (1) surface interactions, and (2) bulk interactions.

The techniques that have been previously used for the study of hydrogen uptake by materials focus on measurement of either of these two areas. The surface adsorption has been measured using photoemission[2]. The bulk uptake has been measured using resistivity techniques[2] and by quartz crystal microbalance (QCM).[3] Both types of experimental techniques are successful in their own right, but to get the entire range of data of both surface and bulk interactions requires that the two types of experiments must be calibrated with respect to each other. Clearly, there should be an advantage to simultaneously measuring both bulk and surface concentrations of hydrogen with one technique.

This work represents a baseline set of experiments to demonstrate an experimental technique that will measure both surface and bulk hydrogen content simultaneously. Elastic recoil detection analysis (ERDA) was used to demonstrate measurements of hydrogen uptake in titanium. The advantage of ERDA is that it can be used to probe deeply into the sample, thus showing concentrations as a function of depth. Subsequently, the kinetics of the uptake interactions can be more easily understood.

Section 2, of this work, describes the experimental apparatus used for the hydrogen exposure experiments. The basic theory of the measurement techniques is detailed in Section 3. A model for data analysis is presented in Section 4. Section 5 presents the experimental results. Lastly, discussion of the results and concluding remarks appear in Section 6.

2. EXPERIMENTAL EQUIPMENT

2.1 UHV Chamber

The UHV (Ultra High Vacuum) Chamber, as pictured in figure 2.1.1, was the primary experimental apparatus. It was connected by way of a differentially pumped beam line to the 2 MV Van de Graaff accelerator. The chamber contained pumping systems capable of vacuum pressures of 10^{-10} Torr after appropriate chamber baking. The UTI mass spectrometer was used for determining relative residual gas concentrations. The sputter gun was used for sample cleaning. The Auger spectrometer determined the surface characteristics. Also, two detectors were used for ion beam measurements. The gas system provided either argon gas for sample cleaning, or hydrogen gas for exposure experiments. The sample location within the chamber was controlled by a Varian 3 axis-goniometer, attached to a sample holder specifically designed for holding thick metal samples.

The pumping apparatus dominated the vacuum system. A mechanical roughing pump brought the chamber pressure down to tens of microns of Hg. A turbo pump, placed in line with the roughing pump, provided pressures down to 10^{-7} Torr prior to baking; furthermore, it provided a method of keeping gas cycling in the chamber during sample cleaning and hydrogen exposure. The ion pump allowed pressures to 10^{-9} Torr, after chamber baking. A gate valve, closed during argon and hydrogen exposures,

prevented ion pump contamination during hydrogen exposure. Lastly, titanium sublimation provided pumping since titanium adsorbed gasses such as hydrogen; appropriate deposition of titanium on chamber walls provided means to attain 10^{-10} Torr.

The UTI mass spectrometer allowed for the determination of the components of residual gas in the chamber. It was useful for determining the source of a leak. For example, when one of the leak valves was not properly closed, argon gas was present in the chamber preventing pressures from reaching 10^{-10} Torr. Using the UTI helped isolate the source of the leak, which led to quick corrective measures. The UTI was also used to verify the purity of the gas sources. For instance, if either the argon or the hydrogen gas were contaminated with water, introduction of the gas in the chamber would defeat the efforts of baking.

Once UHV had been achieved, contaminants were present on the sample in the form of organic material and oxides. These materials needed to be removed from the sample surface so that the surface characteristics would be well defined. All the contaminants previously mentioned could be removed by heating to temperatures higher than 600°C; however, at these temperatures, sulfur would diffuse out of the bulk of the sample onto the surface. Such a situation left undesirable surface conditions, so the sulfur had to be removed. Removal could have been accomplished by heating the sample to the sulfur sublimation point, but, since a titanium phase change exists at a lower temperature, excessive heating was avoided. The removal of sulfur was accomplished using a 2kV sputter gun, which ionized argon gas and accelerated it toward the sample surface, knocking off the surface contaminants as a result of collision. Since the sulfur did not

bind tightly to the surface, one hour of sputtering at a microampere per square centimeter of sample current was sufficient to remove sulfur.

The characteristics of the sample surface were determined by Auger Electron Spectroscopy (AES). Section 3.1 details the theory of AES. Surface characteristics could have been determined throughout the exposure series, but in the interest of maximizing usable concentration data, the AES measurements were confined to the beginning and the end of an exposure series. Once surface characteristics were sufficiently determined to begin an exposure, the AES electronics were shut off to avoid noise in the solid state detectors used for the ion beam experiments.

Two solid state detectors were present in the chamber. The first used a rotating axis, providing the ability to detect reflected particles at any azimuthal direction. It was typically fixed at a scattering angle of 155 degrees, the best possible angle for Rutherford Back Scattering that determined the incident beam energy (see Section 3.2). The second detector used a fixed mount at a scattering angle of 25 degrees, representing a good scattering angle for the forward scattering technique of ERDA, detailed in Section 3.2.

A two-line gas system allowed for the separate use of two different gases, eliminating the possibility of contamination of one gas line with differing gases. Each gas line had its own shut-off valve, regulator, and leak valve; both lines had valves which could be opened for pumping the lines clean with the turbo pump. Periodically, the lines were evacuated and heated to insure contaminant-free gasses. When not in use, the lines typically had higher than atmospheric pressure of gas to prevent atmospheric contaminant gases from entering the system.

Attached to a Varian 3-axis goniometer, a new sample holder was built to handle thick, approximately 1 millimeter, samples (see Figure 2.1.2). Heating the sample was accomplished by electron beam heating, where the sample was put at a high potential and the filament generated thermionic electrons. Careful control of the filament current allowed very precise control of the sample temperature, which was measured using a thermocouple attached to the rear surface of the sample. Temperatures were kept below 750°C to avoid a phase transition of the titanium samples.

Overall, the UHV chamber allowed precise control of experimental conditions, minimizing contaminants. Once ultra-high vacuum conditions were established, hydrogen uptake experiments could be performed using a variety of surface conditions; consequently, UHV became essential to measure any significant uptake.

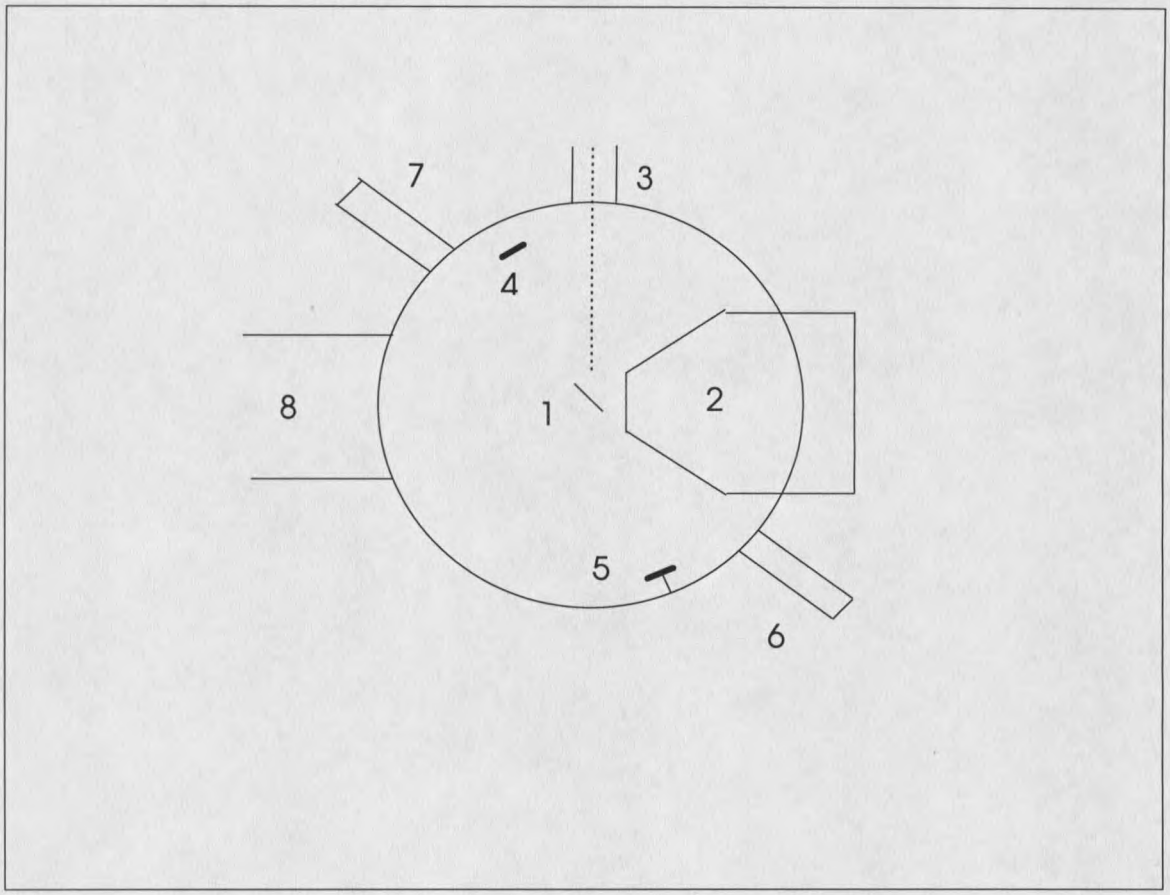

Figure 2.1.1

Schematic of UHV chamber.

(1) The sample, (2) the Auger cylindrical mirror analyzer, (3) ion beam path from accelerator, (4) movable solid state detector for RBS, (5) fixed solid state detector for ERDA, (6) gas system, (7) UTI mass spectrometer, (8) connection to pumps.

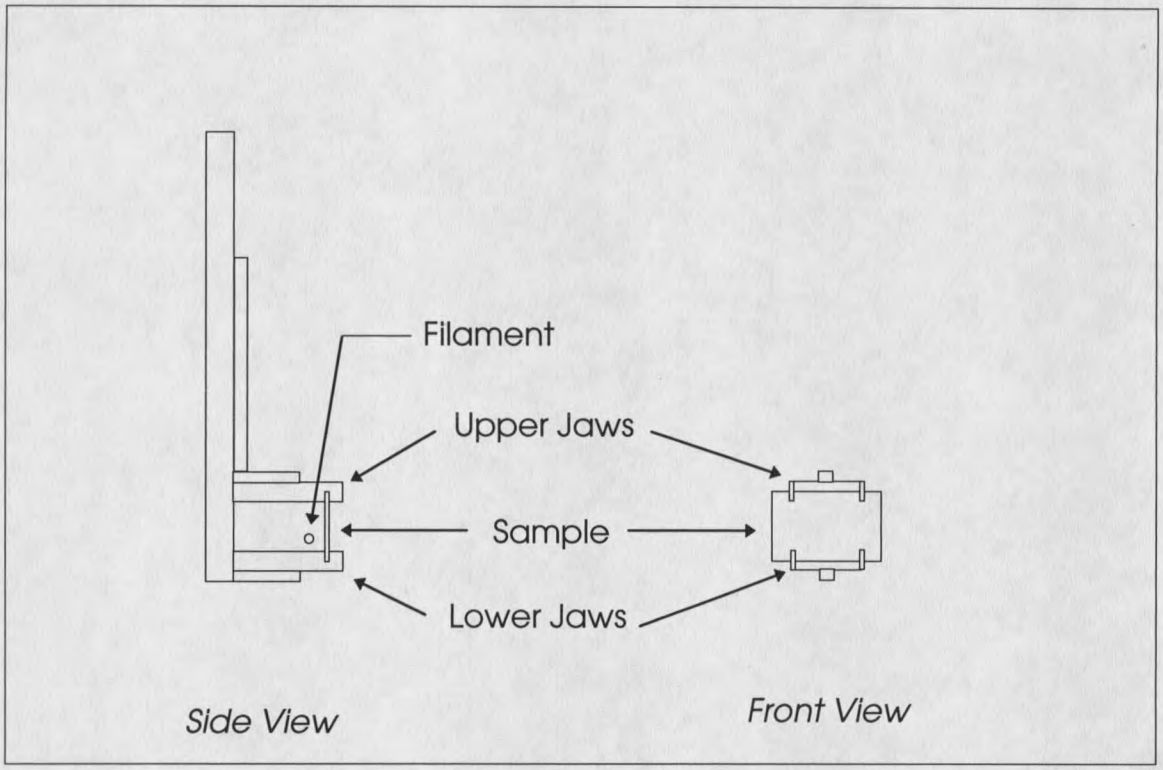

Figure 2.1.2

Schematic of sample holder designed for thick, approximately 1mm, samples. Note that sample heating is accomplished by electron beam heating. The jaws are made of tantalum. The frame is made of aluminum.

2.2 The Van de Graaff Accelerator

The Van de Graaff accelerator provided a source of alpha particles (helium ions) which were used for the ion beam techniques detailed in Section 3.2. The Van de Graaff operates on the principle of static charge separation, where one end of the accelerator is positively charged, the source end. Positive ions were created at the source end, forcing them to accelerate away from the positively charged end. The ions, once leaving the front of the accelerator, entered a bending magnet that allowed ions to be separated by kinetic energy. The magnetic field could be controlled to specifically bring the singly ionized helium down the beam line to the UHV chamber and sample.

Setting up the high potential was accomplished by a belt transporting electrons away from the terminal end of the accelerator apparatus. A simplified picture of a typical Van de Graaff generator (see Figure 2.2.1) proved useful for understanding the principle of operation. The belt was set into rapid rotation. The positively charged source point removed electrons from the belt which in turn removed electrons from the metal dome. Moving electrons to the front of the accelerator, in this manor, allowed for a very large potential difference to exist. Though some accelerators have potentials up to 20 million volts, this Van de Graaff was limited to a potential of 1.9 million volts. A controlled discharge, known as corona discharge, near the dome (not shown) allowed for precise control of accelerator voltage.

If an ionized particle, with charge Ze, was introduced in the interior of the charged

dome, it would move along the electric field generated by the large potential difference. The resulting particle had kinetic energy

$$E_0 = Ze\Delta\phi \tag{2.2.1}$$

at the end of the accelerator. By allowing the ion to pass through the end of the accelerator, a usable source of ions at a kinetic energy as specified by equation 2.2.1 was available.

Unfortunately, because of ionization of residual gases along the acceleration column, many accelerated species were present at the front with varying kinetic energies based upon their level of ionization. Singling out a specific ion species at a particular kinetic energy was accomplished with a bending magnet. Any charged particle that enters a magnetic field with a momentum $p_\perp=(2mE_0)^{1/2}$, perpendicular to the field, will move in a circular path of radius

$$r = \frac{cp_\perp}{|Z|eH} \tag{2.2.2}$$

where H represents the magnetic field strength, determined by current flowing through the magnet coils. Thus, the desired particle of charge Ze and mass m could be delivered down the beam line at the desired energy, E_0.

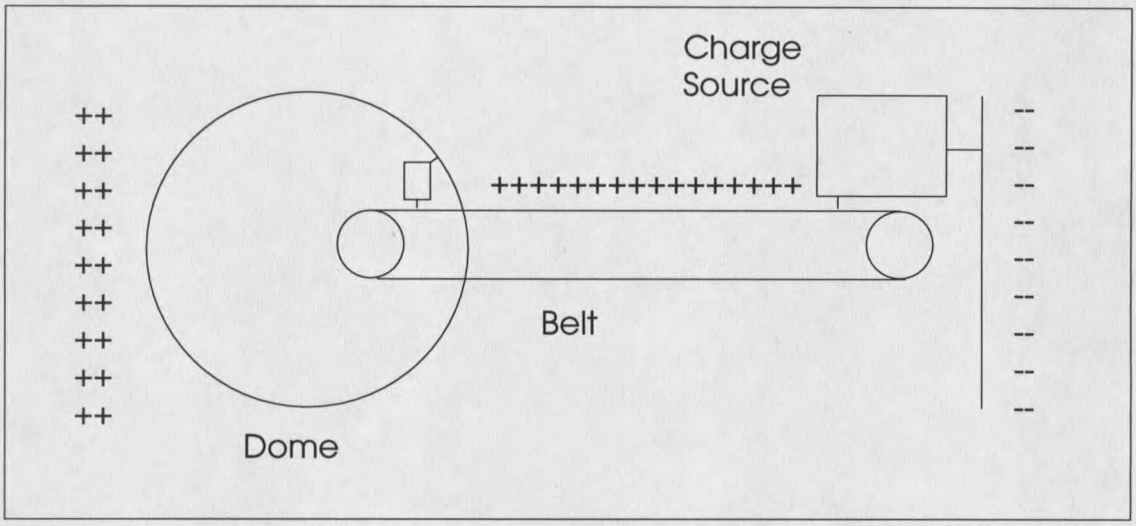

Figure 2.2.1

Schematic diagram of Van de Graaff Generator.

Note that the charge source strips electrons from the belt thereby giving a net positive charge at the dome or terminal end. A beam line may be placed along the axis of the generator, allowing positively charged ions to be accelerated out the front end.

3. THEORY OF EXPERIMENTAL TECHNIQUES

3.1 AES

Auger Electron Spectroscopy (AES), was used to determine the characteristics of the metal surface with respect to the presence and relative concentrations of contaminants. The Auger process is the particle counterpart of fluorescence, since multiple electron atoms can drop an electron down to a lower energy state by freeing another electron instead of emitting a photon. In fact, the Auger decay occurs with higher probability than fluorescence as the number of electrons increases. Thus, the Auger process became a fundamental quantum mechanical process.

Typically, the AES apparatus and data acquisition was straightforward. An election gun ionized the atom, leaving an unoccupied energy state. An analyzer detected the released Auger electron and measured its energy. The analyzer, used for the equipment detailed in Section 2.1, was a cylindrical mirror analyzer (CMA). The CMA operated by selecting an energy for detection and would give a signal based upon the number of electrons incident upon it. By changing the potential on the outer cylinder of the CMA, electrons of corresponding energies were passed to the detector, resulting in an Auger spectrum of intensity as a function of energy [for details of the AES apparatus reference Schaus and Smith[4] or the AES manual[5]].

The basic principles governing the Auger process require that a single electron bound state of an atom be empty. The empty state could be created by any number of

processes, but a common method is by knocking the electron out of the atom by another high energy electron. Once the electron had been knocked out of the atom, there remains a vacancy at the energy level, leaving the atom in an exited energy state (see Figure 3.1.1a). The atom can return to a lower energy state by dropping an electron to the empty state. However, quantum mechanical conservation laws demand that the energy lost by the decaying electron must be gained by another particle. Fluorescence conserves the energy by creation of a photon, but Auger emission conserves the energy by transferring it to another electron, thereby raising it to an even more exited state or freeing it from the atom (see Figure 3.1.1b).

Since the energy states for an element were characteristic to each element, the Auger electrons will be characteristic to the element emitting the electron. The characteristic Auger energies, as presented in Table 3.1.1, depend upon the electron shell of all three electrons involved in the process. Consequently, the KLL Auger process signified an empty K shell being filled by an L shell electron causing the liberation of another L shell electron.

AES energies could be specified by an empirical expression:

$$E_{Z,abc} = E_{Z,a} - E_{Z,b} - E_{Z,c} - \frac{1}{2}[E_{Z+1,c} - E_{Z,c} + E_{Z+1,b} - E_{Z,b}] \tag{3.1.1}$$

with Z representing the atomic number and a, b, and c describing the process, such as KLL.[4] Unfortunately, there exists no analytical formula which gives the resulting Auger energies, since the quantum mechanical representation of the matrix element for multiple electron interactions within an atom requires an analytic representation of a multiple

electron atom that has not been done to date.

Once an Auger spectrum had been taken, the relative intensities of the spectral lines corresponding to the individual elements could be compared to find relative concentrations of those elements on the surface. The relative concentration of an element, defined by

$$C_z = \frac{I_z / S_z}{\sum_j I_j / S_j} \tag{3.1.2}$$

with I being the intensity of a spectral line and S being the sensitivity factor of the same line (see Table 3.1.2 for sensitivity factors of interest), determined the characteristics of a surface.

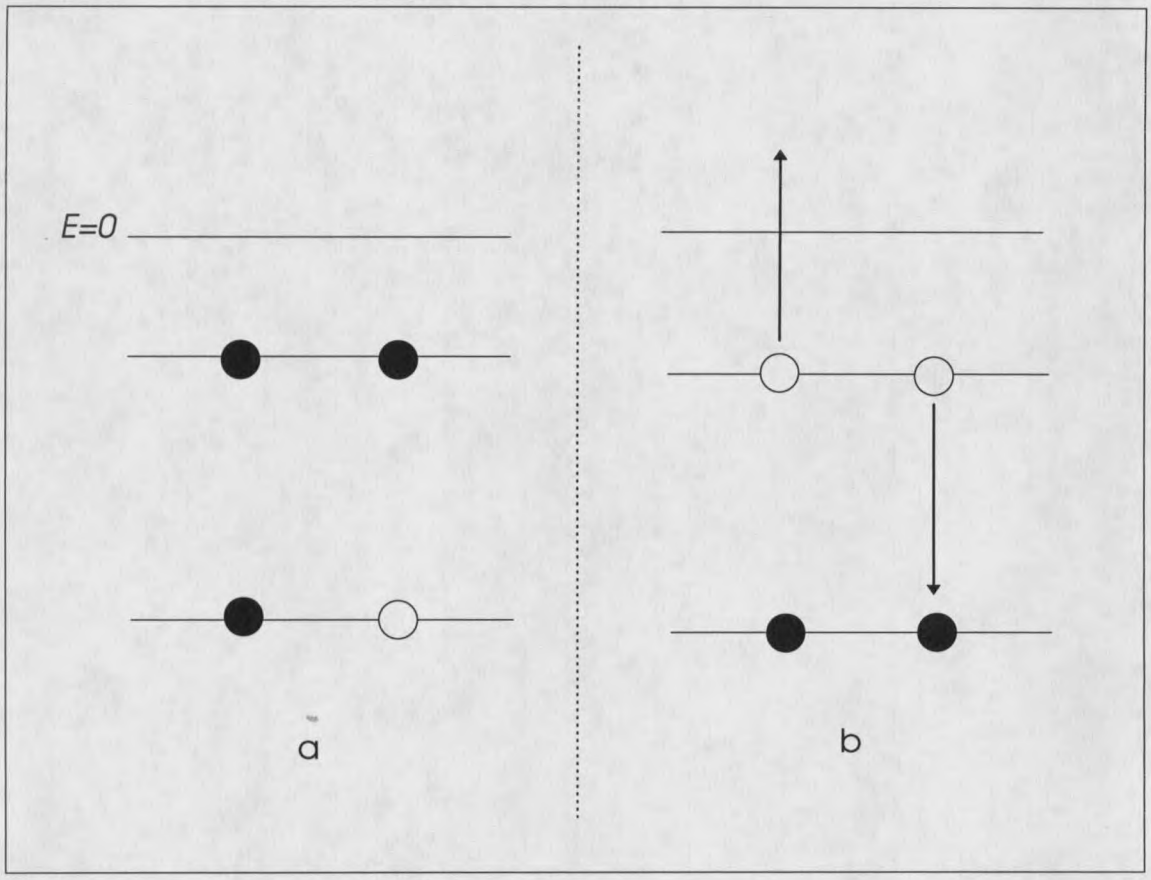

Figure 3.1.1

The Auger Process.

Atom in excited energy state (a) will decay to a less excited state (b) by emitting an electron. Conservation of energy requires that the emitted electron's energy be increased by the amount of energy lost by the decaying electron. Measurement of the energies of Auger electrons will provide a signature of the element which emitted the electron.

Element and Auger Transition Process	Auger Energy (eV)
Titanium, MNN, LMM, LMM	40, 390, 410
Carbon, KLL	270
Oxygen, KLL	510
Sulfur, LMM	150

Table 3.1.1

Auger energies for selected elements and transition processes.[5]

Element and Transition Process	Sensitivity factor
Titanium, LMM	.45
Sulfur, LMM	.8
Carbon, KLL	.16
Oxygen, KLL	.5

Table 3.1.2

Auger sensitivity factors for selected elements and transition processes.[4]

3.2 ERDA

Elastic Recoil Detection Analysis (ERDA), also known as Forward Recoil Spectroscopy (FRS), is a method by which the concentration of an element within a sample may be measured by bombarding the sample with a heavier element of known kinetic energy. For detection of hydrogen in metals, the obvious choice for the heavier element is helium. The collisions involved in ERDA are between charged nuclei, so the cross sections are on the order of 1 barn, 10^{-24} cm^2. Collisions with the electrons present in the sample occur, but the energy and momentum lost in each interaction is small allowing all such interactions to be represented by a stopping rate, energy loss per unit length, for the material that the ion passes. A careful analysis of the collision of the nuclei, using classical physics, leads to a good overview of theoretical considerations involved in ERDA.

Analysis of a classical collision, see Figure 3.2.1 , gives the characteristics necessary for determining parameters to interpret an ERDA spectrum. The collision is considered a completely elastic event between the nuclei of the participant atoms, ignoring the effects of electrons in the interaction. The equations for evaluating the kinematics of the collision are

$$E_0 + E_1 = E_2 + E_3, \tag{3.2.1}$$

from conservation of energy, and the two equations,

$$(2m_0E_0)^{1/2} + (2m_1E_1)^{1/2} = (2m_2E_2)^{1/2}\cos\theta_2 + (2m_3E_3)^{1/2}\cos\theta_3 \tag{3.2.2}$$

and

$$(2m_2E_2)^{1/2}\sin\theta_2 + (2m_3E_3)^{1/2}\sin\theta_3 = 0\,, \tag{3.2.3}$$

from conservation of linear momentum. By fixing θ_2 as the known scattering angle, and noting that the kinetic energy of the target, E_1, is zero, the above equations may be solved for the energy of the particle moving along the known scattering angle, where a detector may be located. So the energy at the detector is given by

$$\begin{aligned} E_2 = & \frac{\left[(m_3 - m_0)(m_3 + m_2) + 2m_0m_2\cos^2\theta_2\right]E_0}{(m_3 + m_2)^2} \\ & \pm \frac{\left[m_0m_2(m_3 - m_0)(m_3 + m_2) + m_0^2m_2^2\cos^2\theta_2\right]^{1/2} 2E_0\cos\theta_2}{(m_3 + m_2)^2}. \end{aligned} \tag{3.2.4}$$

Assuming that there is no mass transfer in the collision, which is reasonable for a classical collision involving atomic nuclei, the masses m_2 and m_3 are either m_0 of the incident particle, or m_1 of the target particle.

There are two important cases for equation 3.2.4. If $m_3 = m_1$, then the energy of the incident helium nuclei can be determined by elastically scattering it off the metal nuclei through a large angle θ_2. Also, the first case determines the energy of forward scattered helium, by small θ_2, when colliding with the metal nuclei. Secondly, if $m_3 = m_0$, then the energy of the forward scattered hydrogen nuclei can be determined from equation 3.2.4.

In the first case, where $m_3 = m_1 = M$ (M being the mass of the metal nuclei) and $m_2 = m_0$, equation 3.2.4 reduces to

$$E_2 = \left[\frac{\left(M^2 - m_0^2 \sin^2 \theta_2\right)^{1/2} + m_0 \cos\theta_2}{m_0 + M} \right]^2 E_0 \tag{3.2.5}$$

where the quantity multiplying E_0 is the kinematic factor, κ, for Rutherford Back-scattering Spectroscopy (RBS).[6] RBS is the method used to determine the incident energy of the helium beam. Using the mass of the metal nuclei making up the sample, M, and the mass of incident helium nuclei, m_0, RBS allows determination of the incident energy through the relation

$$E_0 = E_2 / \kappa \tag{3.2.6}$$

Figure 3.2.2 shows a typical RBS spectrum. The forward edge of the spectrum (a) represents the classically scattered helium atom leaving the surface of the material. Typically, RBS was done at a scattering angle, $\theta_2 = 155^o$, giving a kinematic factor of $\kappa = 0.7172$ for a titanium sample.

Furthermore, the first case allows determination of the forward scattered helium energy at angle $\theta_2 = 25^o$ with respect to the detector. Subsequently, the helium atom which scatters elastically off the titanium surface has energy, $E_2 = 0.9848E_0$, creating a problem that will be specified below.

The second case, where $m_3 = m_0$ and $m_2 = m_1$ (m_1 being the mass of the forward scattered hydrogen atom), reduces equation 3.2.4 to

$$E_2 = \left[\frac{4m_0 m_1 \cos^2 \theta_2}{\left(m_0 + m_1\right)^2} \right] E_0 \tag{3.2.7}$$

where the quantity in square brackets is the kinematic factor, k, for ERDA. Note that the squared cosine makes the best angles of choice to be small. The scattering angle will be further optimized for the scattering cross-section, as shown below.

By comparison, the energy of a scattered helium atom at the detector, as detailed above at $\theta_2 = 25^o$, is $E_{He} = 0.9848E_0$ and the energy of the hydrogen atom forward scattered to the detector, given by equation 3.2.7 at the same angle, is $E_H = 0.5257E_0$. Clearly, the classical scattering event would be adequate for distinguishing hydrogen from helium, based upon the particle energies, but in both cases, the energy measured at the detector is decreased depending upon the depth of the scattering event within the material. The scattered nuclei will lose energy from the multiple collisions with electrons in the material. Unfortunately, this will cause the spectrum for both hydrogen and helium to be spread from zero energy up to the energy of the surface collision, giving overlapping energy spectra and effectively burying the hydrogen spectrum within the helium spectrum.

Using the knowledge of the stopping power, it is possible to remove the helium background spectrum from the hydrogen signal. Building a classical model of the multiple scattering interactions has little practical value; experimental data of the energy loss of particles with well defined energies passing through materials are used to provide a best fit function of energy loss known as the stopping power.[7] Figure 3.2.3 shows the stopping powers for hydrogen and helium within aluminum. Note that for higher energies the helium stopping function is greater than that for hydrogen. Consequently, an

aluminum stopper foil of 8 micrometers may be used to stop helium nuclei from reaching the detector. The hydrogen energy is also decreased, but the particle is not stopped by the foil.

Working backward from the detector, since the energy of the hydrogen is measured, the analysis of the ERDA spectra may begin. Analysis begins at the stopper foil (see Figure 3.2.4). The detector measures the energy of the incoming hydrogen nuclei, E_H. The energy for the hydrogen is

$$E_H = E_{OUT} - \Delta E_s(E_{OUT}), \tag{3.2.8}$$

where $\Delta E_s(E_{OUT})$ is the energy loss due to the stopper foil as a function of energy, and E_{OUT} is the energy of hydrogen leaving the sample.

Unfortunately, the stopper foil also decreases the resolution of the energy measurement. Suppose that a collection of protons enter the stopper foil with energy E_{OUT}. The measured energies of the hydrogen nuclei entering the detector will have a distribution of energies. The loss of energy resolution is known as straggling. References[8,9] present a good theoretical development of straggling effects. In essence, the protons moving through the material along different trajectories encounter non-stationary electrons and target nuclei, and through the collision process, the nuclei lose energy depending upon the impact parameters of the collisions. The variance of the energy, straggling, takes the form

$$\delta(\Delta E_S) = 2(2\ln 2)^{1/2} Z_1 e^2 \sqrt{4\pi N Z_2 t}, \tag{3.2.9}$$

where t is the thickness of the foil, and N is the number density of target atoms in the foil.

Now, moving backward along the particle trajectory in Figure 3.2.4, the next item for characterization is the energy of the hydrogen leaving the sample, E_{out}. The energy of the hydrogen leaving the sample has a maximum value defined by the elastic collision occurring at the surface, $E_{MAXout} = 0.5257E_0$. Consequently, the energies associated with hydrogen originating from beneath the surface will depend upon the stopping power of the sample. Since the hydrogen loses energy coming out of the sample, it is reasonable to assume that the incident helium will also lose energy going into the sample. By combining this into a single energy loss term, then

$$E_{OUT} = kE_o - [S]x, \tag{3.2.10}$$

where x is the depth of the collision and $[S]$ is the stopping power associated with the material. The stopping power $[S]$ has two contributions. The first contribution will be the energy lost by the helium nuclei prior to the collision, and the second will be the energy lost by the hydrogen after the collision. So, the stopping power is given by

$$[S] = \frac{kS_1}{\sin\alpha} + \frac{S_2}{\sin(\theta_2 - \alpha)}, \tag{3.2.11}$$

where S_1 is the stopping power of helium in the material and S_2 is the stopping power for hydrogen in the material. By assuming that the energy lost is small, as a first approximation, then the stopping powers can be evaluated at the surface energies. The stopping power of helium may be written as a function

$$S_1 = S_1(E_o), \tag{3.2.12}$$

and the stopping power of hydrogen may be written as a function

$$S_2 = S_2(E_{OUT}). \tag{3.2.13}$$

Again the stopping power for the material adds to the energy resolution error for the system; however, most of the effects are considerably less than that of the stopping foil so for the deepest portion of the sample, 1000 Å, the stopping foil straggling is still an order of magnitude larger than the straggling associated with the sample.

Finally, the energy measured at the detector as a function of depth may be stated as

$$E_H = kE_0 - \Delta E_S - [S]x, \tag{3.2.14}$$

where the kinematic factor, k is defined by equation 3.2.7, the energy loss due to the stopper foil is a tabulated value, and the stopping power of the sample is defined by equation 3.2.12-13. By solving for x, the depth as a function of energy determined at the detector is found.

The solid state detector used for the ERDA experiment registers counts in a particular channel. The counts are the number of incoming hydrogen atoms knocked out of the sample. The yield, number of counts per channel, of hydrogen at the detector is

$$Y = Q\Omega(\rho\delta x)\sigma \tag{3.2.15}$$

where Q is the number of helium atoms hitting the surface (found through charge integration), Ω is the solid angle of the detector, σ is the scattering cross-section for the collision, and ($\rho\delta x$) is the number of hydrogen atoms per unit area in a slab of thickness,

δx at depth x. Thus equation 3.2.15 may be rewritten as

$$\rho(x)\delta x = \frac{Y}{\Omega Q \sigma}. \tag{3.2.16}$$

Since Y is the yield per channel, $N(E)$ is defined as the yield per keV, and the factor δE is introduced as the energy per channel. The differentials may be grouped together, and their quotient may be defined as some generalized stopping power, being an energy loss per unit length. The generalized stopping power is [S]/0.63 (see Saleh[10] for a detailed derivation), where [S] is the stopping power of the material. The 0.63 comes from the straggling effects of the stopper foil and is dependent upon the thickness and composition of the foil (aluminum foil of 8 μ m in this case). Thus the density of hydrogen within the sample is

$$\rho(x) = \frac{N(E)[S]}{0.63\Omega Q \sigma}. \tag{3.2.17}$$

Together with equation 3.2.14, equation 3.2.17 allows the analysis of an ERDA spectra. A hydrogen concentration versus depth profile may be made. The only issue that needs additional comment is the collision cross-section.

The helium collision with hydrogen may be viewed as classical. Thus as a first approximation the cross-section may be equated to the Rutherford cross-section; however, because helium nuclei kinetic energy, E_0, is in the 1.5-2.0MeV range, the interaction is not strictly classical. At these high energies, the nuclear forces begin to contribute to the cross-section, so it deviates from the classical Rutherford cross-section. Baglin et al.[11] have developed a polynomial expression which closely matches data for the

cross-section at various scattering angles. The polynomial is

$$\ln[\sigma(E,\theta)] = aE + b + cE^{-1} + dE^{-2}, \tag{3.2.18}$$

where the coefficients *a, b, c,* and *d* are functions of the scattering angle. Equation 3.2.18 combined with the appropriate coefficients (see Baglin et al.[11] Table 1) give a scattering cross-section which is up to nearly twice the Rutherford cross-section for the energies of interest. Such a deviation is significant for determining accurate concentrations of hydrogen.

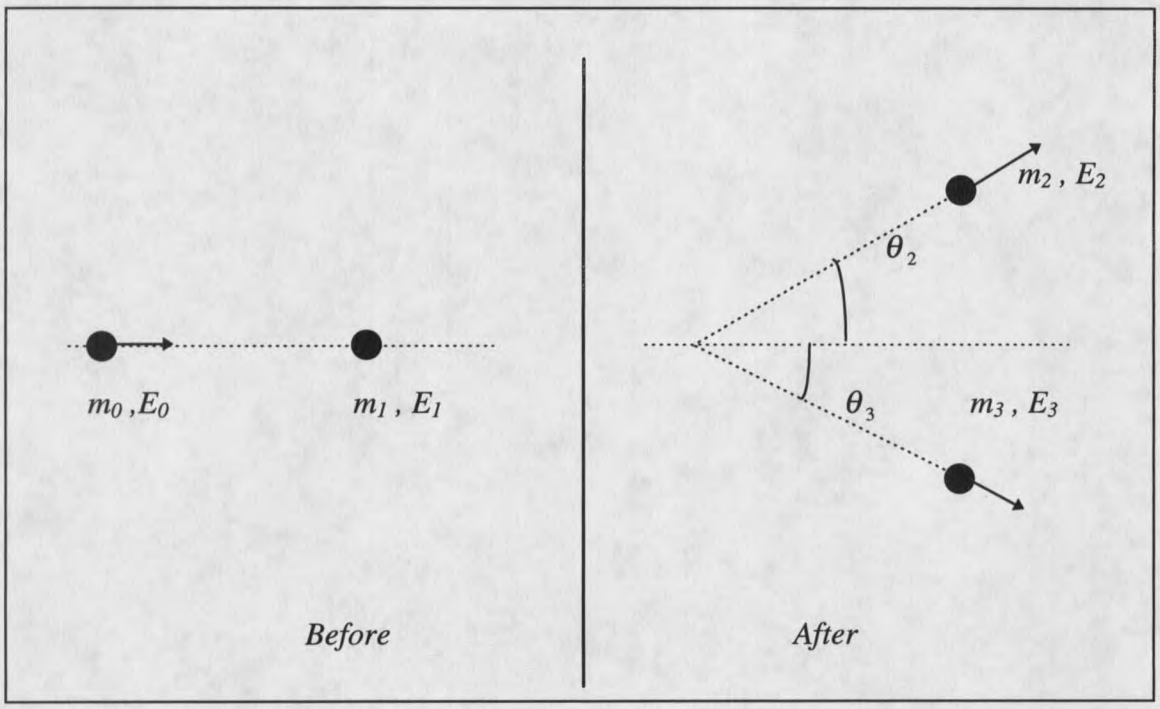

Figure 3.2.1

Classical collision between two point particles..

Note that m_2 can be either m_0 or m_1.

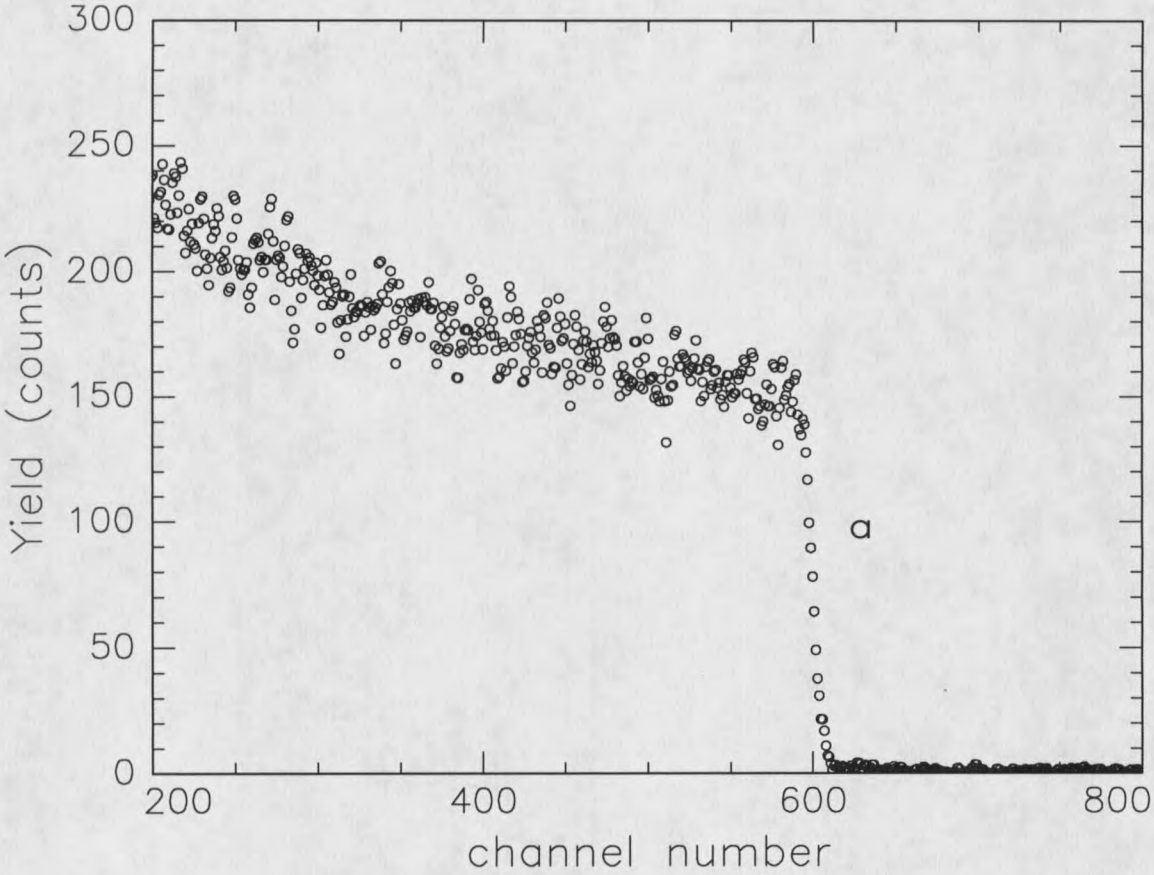

Figure 3.2.2

RBS spectrum for titanium at a scattering angle of 155°.

The channel numbers represent 2keV per channel, so the forward edge (*a*) has an energy of 1.2MeV. Consequently, the incident energy E_0 is 1.67MeV.

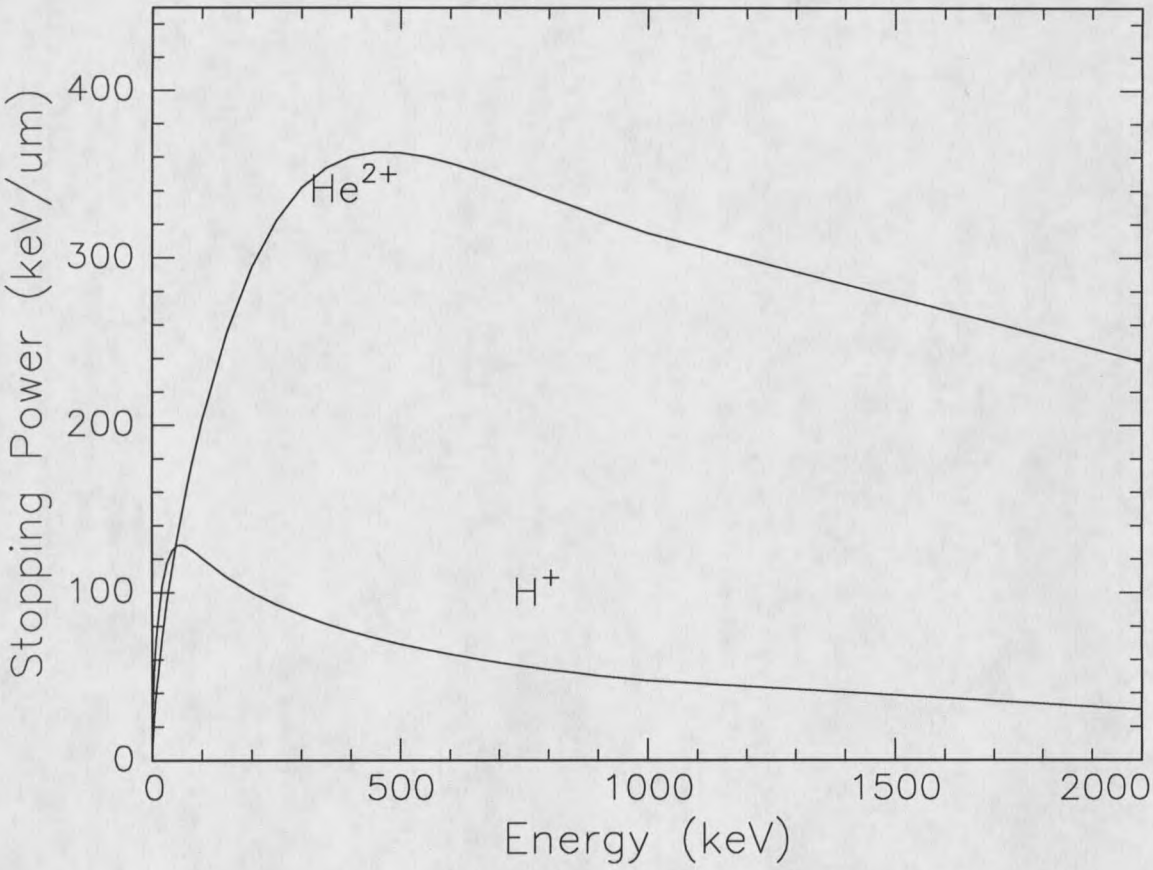

Figure 3.2.3

Stopping powers of hydrogen and helium in aluminum[12,13].

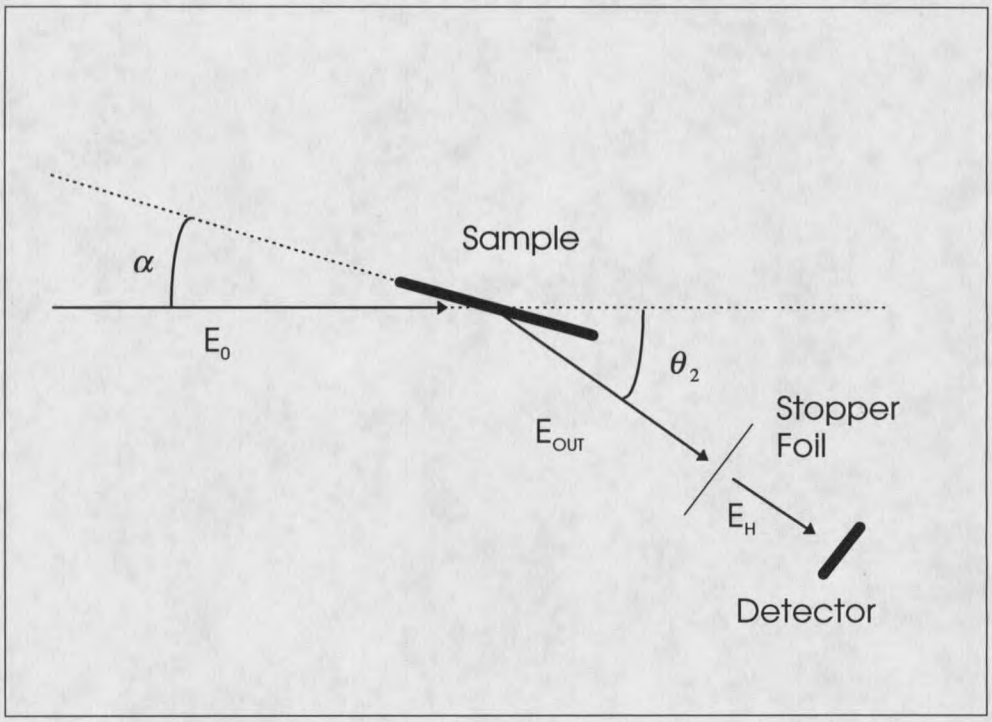

Figure 3.2.4

Schematic representation of ERDA.

4. THEORY OF HYDROGEN ABSORPTION IN METALS

To determine the kinetics of hydrogen absorption on polycrystalline titanium, an existing model presented itself as a reasonable starting point. The model, originally developed by Davenport et al.[14] for explaining photoemission data of hydrogen in niobium and palladium, consisted of a two stage kinetic model; subsequently, the Davenport paper was the primary reference for the discussion which follows. The model considered both the surface concentration and the bulk concentration of hydrogen; consequently, the potential controlling the absorption of hydrogen had a deep well at the surface and a barrier separating the surface from the bulk. Characterization of the barrier determined the behavior of the system. If the barrier was high, hydrogen concentration on the surface would saturate rapidly, leaving the bulk concentration to slowly increase toward saturation; however, if the barrier was low or non-existent, the surface concentration would remain low and would increase only as the bulk concentration increased.

The structure of the potential, as presented in Figure 4.1, determined the behavior of the system. The first potential well, looking into the surface, is associated with surface sites for the binding of atomic hydrogen, with E_D, the desorption energy, being the energy required to remove hydrogen from the surface of the metal. Continuing into the surface, a potential barrier could be encountered that represented a hypothetical difficulty for hydrogen to penetrate into the bulk region. It could represent the breaking of the hydride bonds with the metal to move away from the surface region, or the mechanical strain of

the metal lattice preventing the atoms of hydrogen from moving freely into the bulk. The barrier height, E_A, was defined as the energy measured from the bottom of the surface well. Beyond the barrier would be the region where hydrogen can be in solution, moving freely throughout the bulk. E_S was defined as the solution energy for the atomic hydrogen in the metal, and E_B was the barrier height relative to the solution energy. The solution energy is constrained to obey

$$-E_A + E_B + E_D = E_S, \tag{4.1}$$

allowing for the barrier to vanish, $E_A = E_B$, and thereby forcing the solution energy to be equal to the desorption energy.

Allowing the hydrogen to flow in both directions in the potential well, the following coupled differential equations resulted:

$$\frac{d\Theta}{dt} = 2K_l(1-\Theta)^2 - K\Theta^2 - \nu\Theta + \beta(1-\Theta)x, \tag{4.2}$$

and

$$N_l\frac{dx}{dt} = \nu\Theta - \beta(1-\Theta)x, \tag{4.3}$$

where Θ was defined as the fractional number of allowed sites occupied by hydrogen in the surface region, and x was the fractional concentration of hydrogen in the bulk region. Terms involving Θ^2 require that two hydrogen atoms come together to form a hydrogen molecule. Terms with x and Θ involve interactions between bulk and surface regions. The coefficients K_l, K, ν, and β are dependent upon the energies defined above, and will be further defined to reflect the physical processes involved with the transport of hydrogen between the regions.

The first term of equation 4.2 represented the hydrogen hitting and sticking on the surface; consequently, the coefficient, K_I, should have information concerning the sticking coefficient and the conditions of the hydrogen gas outside the material. Thus, from kinetic theory,

$$K_I = \frac{S_0}{n_s}\left[\frac{P}{(2\pi\, m_{H_2} k_B T)^{1/2}}\right] \tag{4.4}$$

with S_0 as the sticking coefficient, n_s as the number of substrate atoms per unit area, and $P/(2\pi m_{H2} k_B T)^{1/2}$ as the flux of hydrogen molecules at the surface.

The second term of equation 4.2 represents the desorption of hydrogen from the surface to the vacuum outside the material; consequently, K was defined as the desorption rate obeying

$$K \sim K_0 e^{-E_D/k_B T}, \tag{4.5}$$

with K_0 assumed to be 10^{13} attempts per second, representing an attempt frequency of hydrogen trying to escape from the surface.

The third term of equation 4.2, which happened to be the negative of the first term of equation 4.3, was developed as the rate of surface hydrogen going into the bulk; similarly, the fourth term of equation 4.2, which happened to be the negative of the second term of equation 4.3, defined the rate of bulk hydrogen returning to the surface. Using the coefficient K as a model, the coefficients in 4.3 were defined as

$$\nu = \nu_0 e^{-E_A/k_B T} \tag{4.6}$$

and

$$\beta = \beta_0 e^{-E_B/k_B T} \tag{4.7}$$

with the prefactors ν_0 and β_0 defining the attempt frequency at the inner barrier. In the development of the theory, ν_0 and β_0 would be considered free parameters to be adjusted as needed; however, for simplicity, ν_0 and β_0 were considered similar to the parameter K_0, being related to the hydrogen vibrations in the lattice. Therefore, the parameters ν_0 and β_0, as a first approximation, were set equal to K_0.

With the assumed values of ν_0 and β_0, the measurements of the bulk and surface concentrations may be fitted to equation 4.3 by adjusting the energy for the barrier, using tabulated values of E_S and E_D and using the constraint of equation 4.1. Since the barrier energy height, E_A, represented the only free parameter for the bulk fit, determining the height characterized the bulk uptake properties. If the model matches the bulk behavior, then E_A should be within an order of magnitude of the solution energy and the desorption energy. Furthermore, if the barrier height exceeds the desorption energy, careful consideration of the physical processes involved must be made before accepting the model. Another possible outcome was the barrier having a negative value, being deeper than the surface well, or E_B forming an intermediate step potential between the surface and bulk regions, which would suggest that the model should incorporate a region between the bulk and surface having different behavior than either the bulk or the surface regions.

If the barrier energy was suitable for continuing the analysis of the model, the surface data could be analyzed. Since the barrier energy was found, equation 4.2 had a single free parameter, the sticking coefficient, S_0. Clearly, the sticking coefficient represented the physical process of adsorption onto the metal surface. The hydrogen

molecule had to strike the surface in such a way as to be split into atomic hydrogen and be bound to the surface. It was not clear that the sticking coefficient should be constant because of various considerations. First, the hydrogen concentration on the surface could adjust the value of S_0 in a manner that is not represented by the $(1-\Theta)^2$ factor; consequently, a possibility existed that the presence of hydrogen interfered with some of the other possible binding sites as to make sticking more or less likely. Second, the presence of contaminants on the surface should affect the sticking coefficient. Some of the possible hydrogen sites could be taken by other elements; consequently, the contaminant may not only be preventing the hydrogen from sticking to the site, but it may strain the surface to promote or prevent the use of other sites. Third, the presence of contaminants may involve a two stage process which changes the sticking coefficient. Oxygen was known to react with titanium and form stable oxides at room temperature; however, hydrogen had been used to reduce the oxygen from the surface,[15] freeing the site for possible hydrogen adsorption. If the process required freeing oxygen from TiO_2 by forming water, then it required two hydrogen molecules to form the water and another molecule to fill the sites; such a process would definitely result in a non-constant sticking coefficient, especially if reduction of the TiO_2 were easier to accomplish than sticking hydrogen to the surface. Lastly, there could be some dependence upon the bulk concentration, such as straining the lattice so as to promote or prevent sticking; however, such a dependence might be more appropriate for very high bulk concentrations, which were never attained.

The previous considerations were used when compiling results and making

conclusions. Indeed, the values of the barrier energy, E_A, and the sticking coefficient, S_0, represented the physics of the process. Careful consideration of the physical processes involved made for an easier interpretation of results presented in sections 5 and 6.

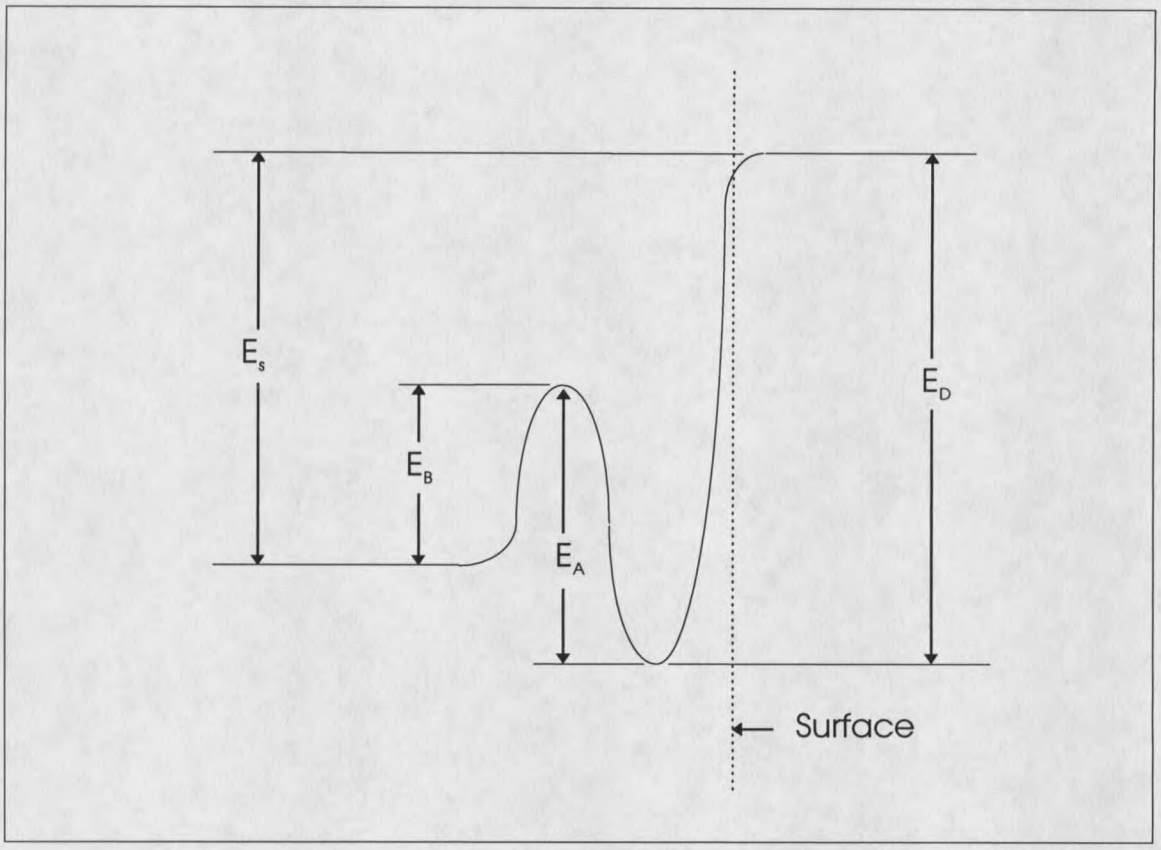

Figure 4.1

Model of potential well for hydrogen absorption into metal surfaces.[14]

5. EXPERIMENTAL RESULTS

5.0 General Information

Once experiments were completed, the ERDA spectra were in the form of counts versus channel number. Using the theory detailed in section 3.2, a program was written to convert spectra into an atomic density of hydrogen versus depth within the titanium sample. The program was written in C++ to take advantage of object oriented design, which developed reusable routines for future data analysis.

In a typical uptake experiment, the sample was exposed to a known pressure of hydrogen for a known period of time. The exposure unit, the Langmuir, was a convenient choice, since it represents microTorr seconds of exposure and the exposure pressures ranged from tenths to tens of microTorr. Two exposure methods were used: (1) exposing for a short time then doing ERDA with the hydrogen removed (variable), and (2) exposing continuously while doing the ERDA (continuous). Both methods were represented within the results.

Converting the series of ERDA spectra to relative concentrations was accomplished by integrating over certain ranges of depth. The boundary was chosen arbitrarily at 1000Å below the sample surface, since experience had shown that the ERDA surface peak appeared entirely within this distance of the surface. All hydrogen deeper than 1000Å was considered bulk hydrogen, and the hydrogen within 1000Å was considered

surface hydrogen. The atomic fractions present were determined by considering the bulk concentration as a total hydrogen density divided by the titanium density throughout the 1000Å of the slab.

The surface hydrogen was assumed to be confined at the surface, thereby making the total surface concentration divided by the titanium concentration in a thin slab the definition of the fractional surface density. The thin slab was considered the average thickness of a unit cell of single crystal titanium, since the surface could be considered microscopic crystals arranged in random orientation. The model developed in section 4.0 required that the maximum value of the surface fractional concentration be one, but the stable hydrides of titanium allowed for a two to one ratio of hydrogen to titanium as a maximum, requiring the fractional hydrogen concentration to become a fractional number of occupied sites within the lattice.

The density of titanium metal is 4.51 g/cc, so the atomic density is 5.67×10^{22} atoms/cc. Thus, the fractional concentration in 1000Å of material was defined by

$$x = \frac{1}{5.67x\,10^{22}\,atoms/cm^3\left[s_{MAX} - 1000x10^{-8}\,cm\right]} \int \rho_H(s)ds \qquad (5.0.1)$$

with $\rho_H(s)$ defined as the hydrogen concentration profile determined from the formulas in section 3.2, with the limits of integration being between 1000Å and the maximum probing depth represented in the ERDA spectrum, and with the coefficient as one over the integral of the titanium atomic density over the same limits.

A titanium crystal has a hexagonal structure (see Figure 5.0.1). Assuming that the surface has a random orientation of the unit cell and the unit cell dimensions were 2.95Å

between nearest neighbor atoms within a plane and 2.35Å between the planes, the average orientation had a depth of 2.61Å. The cross sectional density of titanium within this depth was 1.48×10^{15} atoms/cm^2; consequently, the fractional concentration at the surface became

$$\Theta = \frac{1}{1.48 x\, 10^{15}\, atoms / cm^2} \frac{1}{2} \int [\rho_{total}(s) - \overline{\rho_{bulk}}(s)] ds \qquad (5.0.2)$$

with the average surface concentration being calculated by subtracting the background average bulk concentration from the total concentration (see Figure 5.0.2).

The time axis, with respect to equations 4.2 and 4.3, was determined by dividing through by the pressure of the particular hydrogen exposure, taking into account that ionization gauges read only one-half the actual amount of hydrogen present in the chamber. Once the time axis was in place, best fit functions for the bulk data and the surface data were attempted. The functions were further differentiated to determine rate for bulk and surface uptakes. The data sets were then analyzed with equations 4.2 and 4.3, resulting in experimental values for the barrier height and the sticking coefficient.

As supplemental information, AES spectra were included to characterize the surface conditions before, sometimes during, and after an exposure series. As mentioned in Section 4, a heavy dependence upon surface contaminants could have been present in the sticking coefficient.

The results which follow represented the characteristic uptake of hydrogen by titanium and demonstrated the ERDA technique for studying the absorption phenomena.

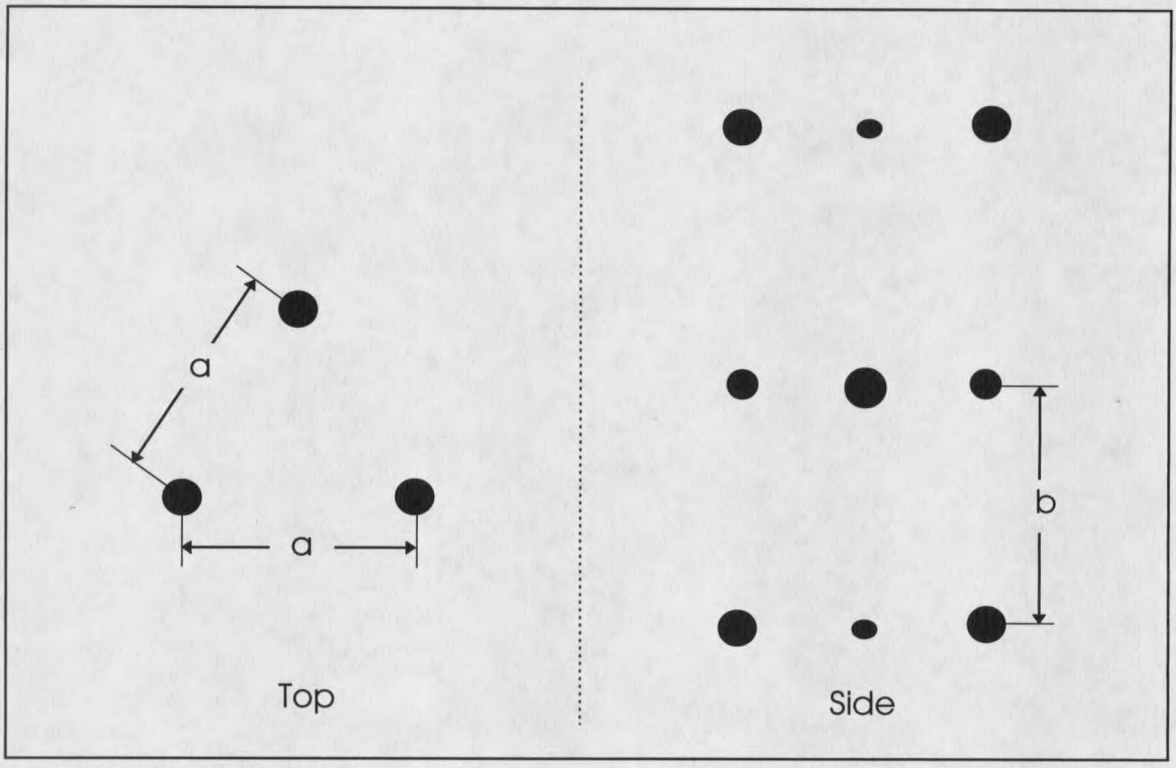

Figure 5.0.1

Hexagonal structure of titanium crystal.

The dimensions are a=2.95Å and b=2.35Å.

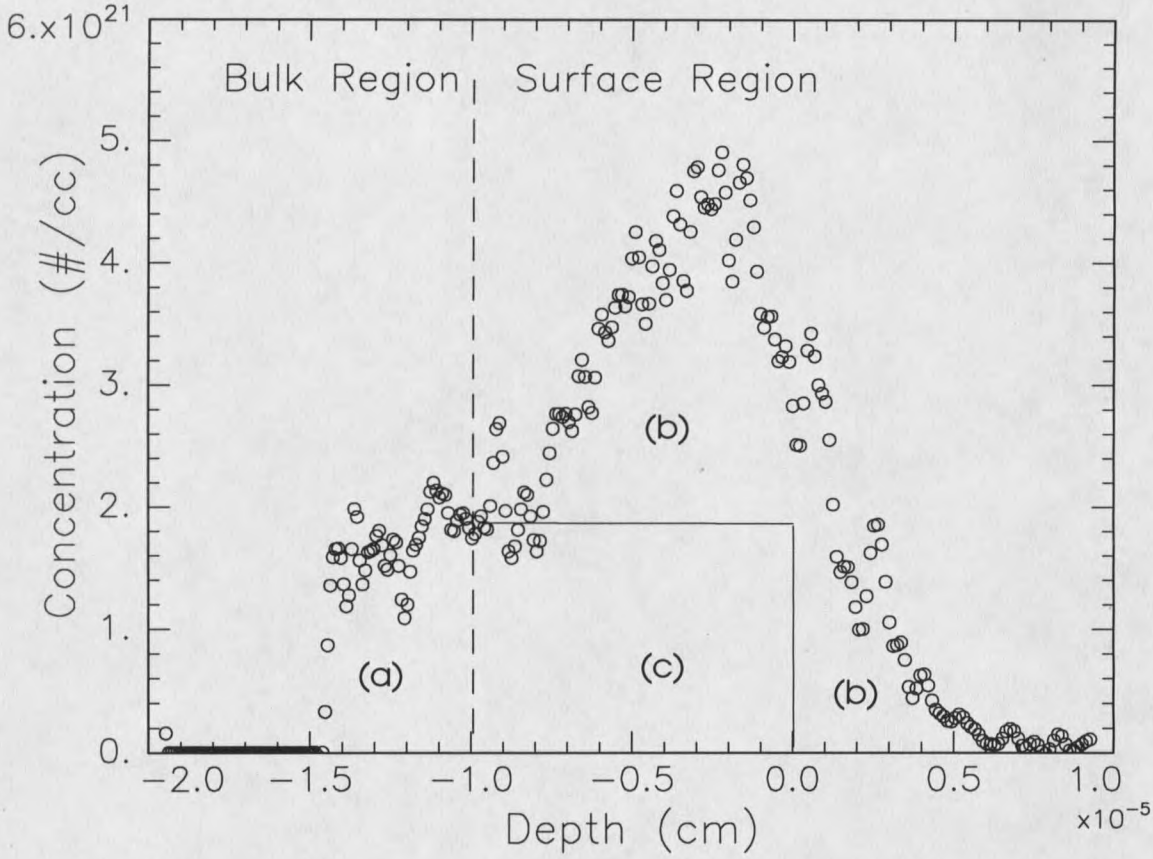

Figure 5.0.2

ERDA spectrum divided into the three regions of interest.

(*a*) Bulk concentration. (*b*) Surface concentration at the sample surface. (*c*) Bulk concentration subtracted from the surface region's concentration.

5.1 UHV, Variable Pressure Hydrogen Exposure Experiments

Experiments were conducted on the 28th of March and 2nd of April 1996 on a relatively clean sample with chamber base pressures of about 1×10^{-9} Torr. As opposed to the continuous hydrogen exposures that would be done later, the first experiments exposed the sample to a small amount of hydrogen, then ceased the exposure in order to return to the base pressure to perform ERDA. Some of the resulting spectra were further scrutinized by taking AES measurements to determine if the exposure changed the surface compositions.

Each exposure, at various hydrogen pressures, took between two and five minutes to complete; subsequently, ERDA measurements were taken immediately afterward to minimize any possible desorption. To establish a baseline of experimental procedures and results, a similar exposure experiment using a quartz crystal microbalance (QCM) was chosen as a method of comparison.[16] The QCM experiment had measured hydrogen exposure on a 1000 Å thin film of titanium at pressures from 10^{-6} to 10^{-5} Torr for 500 seconds; subsequently, the resulting hydrogen uptake indicated continuous absorption but no signs of saturation. In fact, the absorption was nearly linear with respect to time. Consequently, the hydrogen exposures chosen for the variable exposure experiments were an attempt to match the QCM results, which included a range of 0 to 500 Langmuirs.

The March 28th exposure series represented the first series to be done once the preliminary preparations were made. Even though there were some procedural

difficulties, a satisfactory series of spectra leading to near saturation concentrations was developed (see Figure 5.1.1).. The saturation was considered complete since hydrogen concentrations measured at hydrogen exposures of 500 and 1000 Langmuirs did not show any significant change. Furthermore, the values of the data suggested incorrectly that the top layer had exceeded TiH_2 hydrogen concentrations. One explanation is that the fractional surface concentration approached one, giving an experimental error of 20%. Since the exposure series had been stopped at 1000 Langmuirs, there is no way of knowing from the data set whether or not saturation had been achieved. If it was not saturated, thereby continuing to increase beyond the maximum, then the model is only salvageable by redefining the surface region as being two monolayers thick, where hydride is being formed in the second layer. Thus the fractional concentration would be half of the previous value. If this were again to show a definite increase of coverage beyond the point of saturating two layers then the Davenport model must be reconsidered in favor of a model which has the hydride forming layer by layer into the material.

Subsequently, data analysis was confined to realizing that the exposure had reached the saturation point. Furthermore, the variable exposure pressures made it impossible to reasonably determine concentrations as a function of time, indicating that it would not be useful to determine barrier heights and sticking coefficients in this case. It was noted that the concentration is not simply a function of total exposure, but the concentrations have pressure and time dependence.

Similarly, the April 2nd exposure series was conducted in the same manor, except that not as many low exposure spectra were collected (see Figure 5.1.2). By contrast, all

of the April 2nd exposure series data values did not have fractional surface concentration values greater than one.

The surface condition of the titanium sample in the March 28th exposure series, as presented in Figures 5.1.3, show that despite the exposure, the overall surface condition remained the same (AES data for April 2nd series was not available). It was interesting to note that the AES spectrum taken after an exposure had much more noise, despite the equivalent smoothing; consequently, the hydrogen gas must have partially contaminated the AES apparatus.

Both the surface and bulk fractional concentrations have logarithmic dependence with respect to exposure. The curves in Figures 5.1.1 and 5.1.2 represent best fit functions with respect to exposure, defined by

$$x = a_0 \log(a_1 L + a_2) + a_3 \tag{5.1.1}$$

for the bulk, and

$$\Theta = b_0 \log(b_1 L + b_2) + b_3 \tag{5.1.2}$$

for the surface, with a and b being coefficients to be fit. The coefficients for the best fits of the function that the Genplot software accomplished are presented in Table 5.1.1. Beyond this point, analyzing the data with the Davenport model was impossible because of the pressure dependence. Since exposure is defined by

$$L = Pt, \tag{5.1.3}$$

then changes in exposure will be

$$dL = Pdt + tdP, \tag{5.1.4}$$

leaving time derivatives of concentration a poorly defined function because of the

variable pressure.

Overall, the hydrogen exposure series of March 28th and April 2nd represented an uptake to a near saturation point; however, titanium possesses a number of stable hydrides, depending upon the relative concentration of hydrogen to titanium. For the April 2nd series, the surface fractional concentration approached 0.83. Since the fractional surface concentration represents the number of available sites, the ratio of hydrogen to titanium was 1.66 or 5 hydrogen to 3 titanium. In the case for the March 28th series, the ratio approached 2.2 or nearly 2 hydrogen to 1 titanium. Therefore, with surface concentrations being measured with ERDA, hydride formation was inferred.

March 28th Series		April 2nd Series	
$a_0 = 1.73\text{x}10^{-4}$	$b_0 = .223$	$a_0 = 2.1\text{x}10^{-4}$	$b_0 = .166$
$a_1 = .545\text{x}10^{16}$	$b_1 = .465\text{x}10^{17}$	$a_1 = .12\text{x}10^{18}$	$b_1 = .75\text{x}10^{18}$
$a_2 = -.291\text{x}10^{16}$	$b_2 = -.921\text{x}10^{16}$	$a_2 = -.35\text{x}10^{17}$	$b_2 = -.25\text{x}10^{19}$
$a_3 = -2.10\text{x}10^{-3}$	$b_3 = -3.23$	$a_3 = -3.35\text{x}10^{-3}$	$b_3 = -2.53$

Table 5.1.1

Fitting coefficients for logarithmic functions.

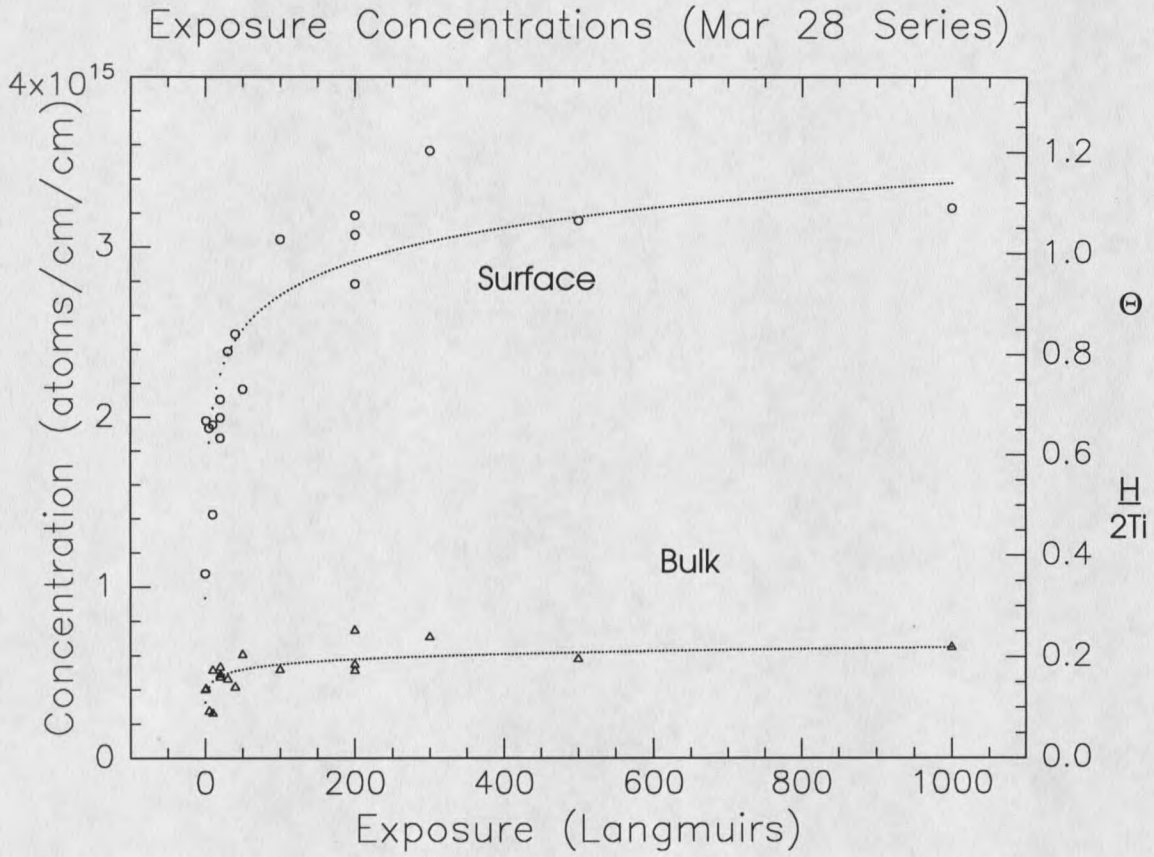

Figure 5.1.1

March 28th exposure series.

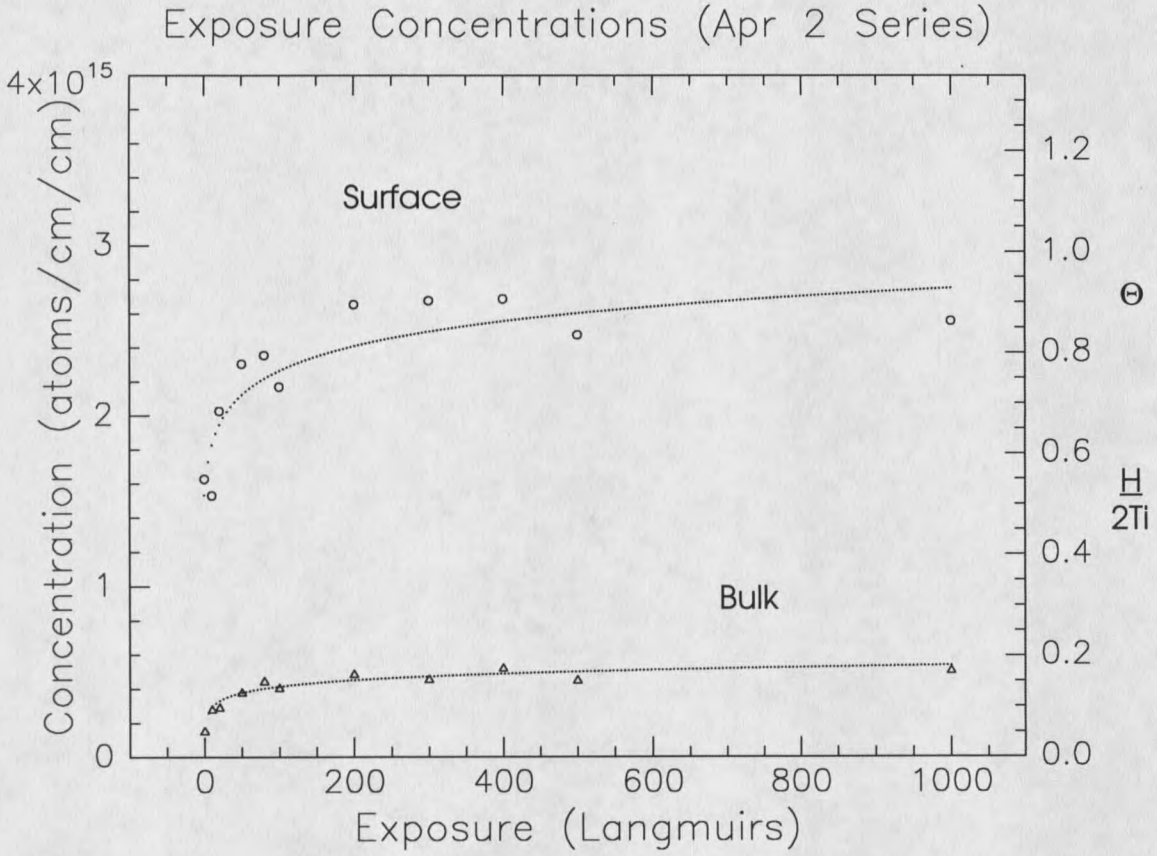

Figure 5.1.2

April 2nd exposure series.

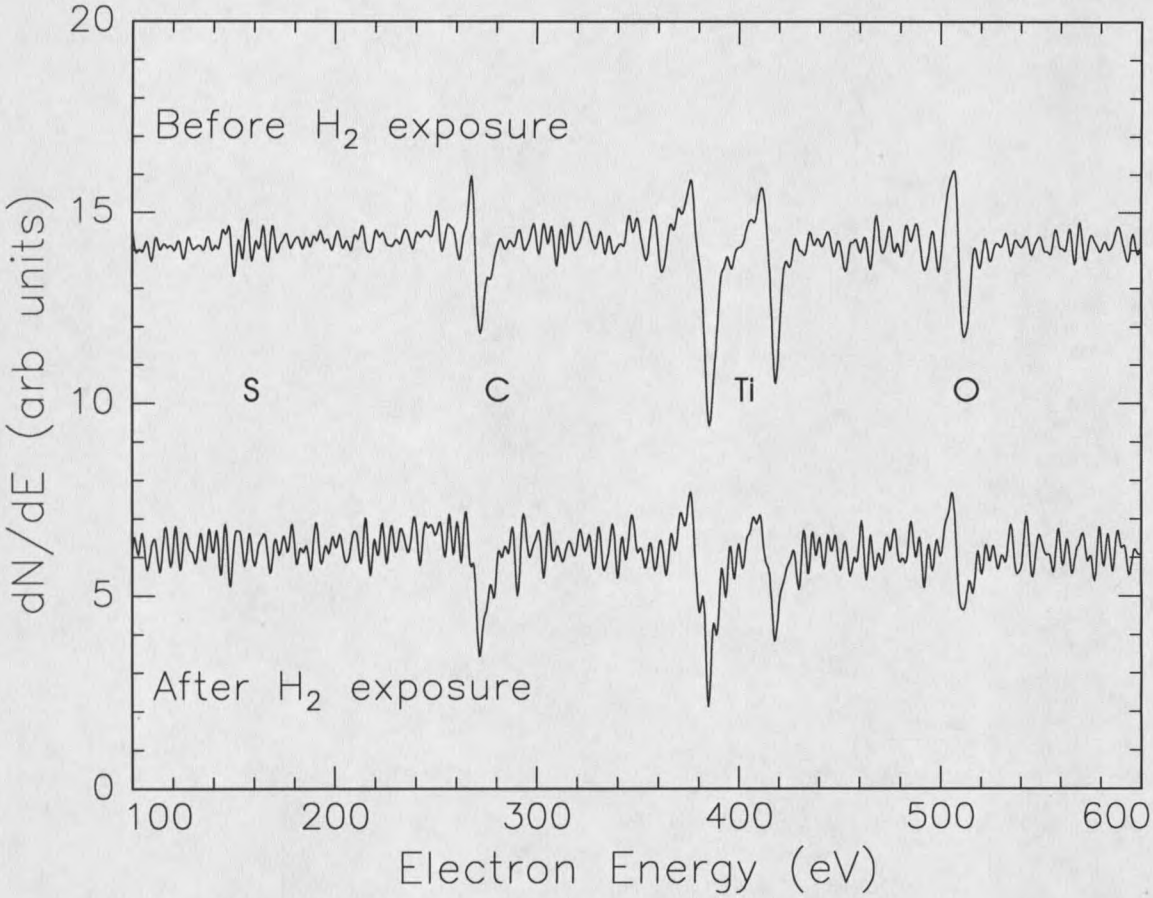

Figure 5.1.3

AES of titanium surface for March 28th exposure series.

Note that the relative concentrations have not changed.

5.2 UHV, Continuous 10^{-5} Torr Hydrogen Exposure Experiments

Experience from the previous experiments at variable exposure suggested that surface saturation had been reached; consequently, the behavior beyond saturation was examined. In the subsequent experiments, hydrogen was exposed to titanium at a continuous pressure in the 10^{-5} Torr range while doing the ERDA. The intent was to observe the behavior once saturation concentrations had been achieved on the surface.

The Jun 25 hydrogen exposure series was accomplished in a baked UHV chamber with a base pressure of 10^{-9} Torr. The hydrogen was exposed to the chamber at $2x10^{-5}$ Torr of pressure. Prior to the exposure series, the sample was sputter cleaned at approximately 400 degrees C for one hour, with AES being done afterwards. A single ERDA spectra was taken prior to the hydrogen exposure to be used as a baseline for the data. Once hydrogen gas had been introduced into the chamber, ERDA spectra were taken back to back throughout the exposure. The sample was exposed to hydrogen for a total of 1 hour and 58 minutes.

Hydrogen uptake was detected (see Figure 5.2.1), as evidenced by increases in both bulk and surface concentrations. It is clear that the surface hydrogen had not saturated at the surface then migrated inward, since there is no apparent width change of the surface peak. Such a situation resulted in treating the surface hydrogen as being at the surface. Consequently, the analysis proceeded accordingly.

The bulk hydrogen concentration varied linearly with time (see Figure 5.2.2). The

fractional concentration changed at an average of 1.19×10^{-7} per second. The resulting rate of change, together with the values for bulk and surface fractional concentrations, resulted in the energy barrier height 0.258eV over the range of the data (see Figure 5.2.3). Consequently, the model presented in section 4 suggests that the interior energy barrier adequately explained the kinetics of the uptake.

Similarly, the surface hydrogen concentration varied linearly with time. The fractional surface concentration changed at an average of 2.06×10^{-5} per second. The resulting rate of change combined with the results for the bulk fractional concentration, resulted with values for the sticking coefficient, S_0, ranging from $.95 \times 10^{-6}$ at the beginning of the exposure to 1.5×10^{-6} at the end of the exposure (see figure 5.2.4). (It was interesting to note that desorption did not contribute to the calculation for the sticking coefficient, since kT was much less than the desorption barrier height.) The fact that a clean surface should have a sticking coefficient of 0.17 indicated that the surface had contaminants[16]. Furthermore, the change of the sticking coefficient suggested that the hydrogen exposure had removed some of the contaminants.

Subsequently, the Auger spectrum, taken before beginning the exposure, showed the existence of contaminants on the surface (see Figure 5.2.5). Primarily, sulfur, carbon, and oxygen were present; however, the Auger spectrum taken after the hydrogen exposure showed no signs of sulfur. It appeared that the hydrogen had been responsible for removing the sulfur from the surface. The relative concentrations of the contaminants, as detailed in Table 5.2.1, indicated that an overall change in the composition of the surface contaminants had occurred.

Though saturation had not been accomplished, the results indicated some unusual behavior. Both the surface and bulk concentrations increased linearly at different rates, which suggested that the surface concentration was not controlling the bulk rate of uptake. Such a situation would suggest that surface fractional concentrations of 0.30 are insufficient to reduce bulk uptake rates, but the differing rates of uptake indicate that the surface adsorbs hydrogen faster than it is transported into the bulk.

Element	Relative concentration	
	Before exposure	After exposure
Titanium	.260	.283
Sulfur	.053	.026
Carbon	.610	.559
Oxygen	.069	.133

Table 5.2.1

Relative concentrations of sample surface.

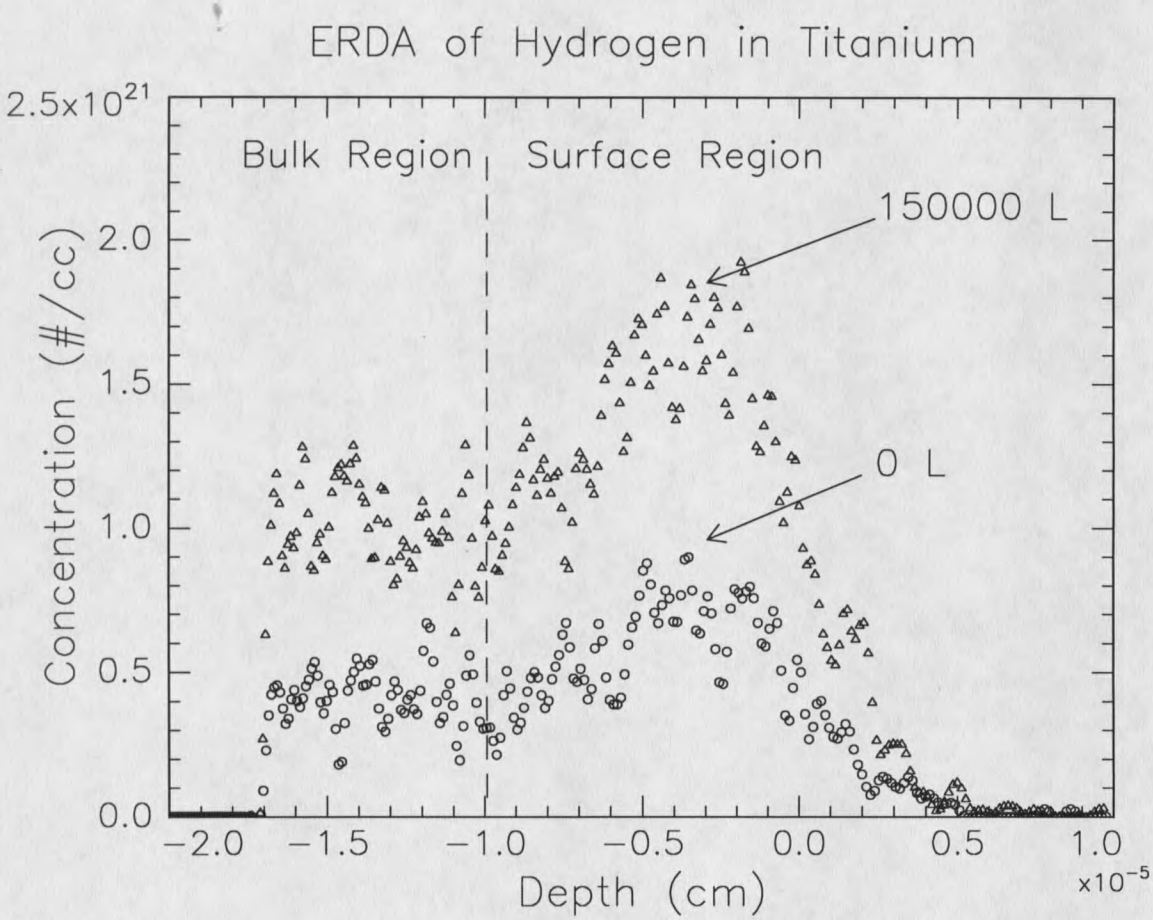

Figure 5.2.1

ERDA of hydrogen in titanium at two different exposures.

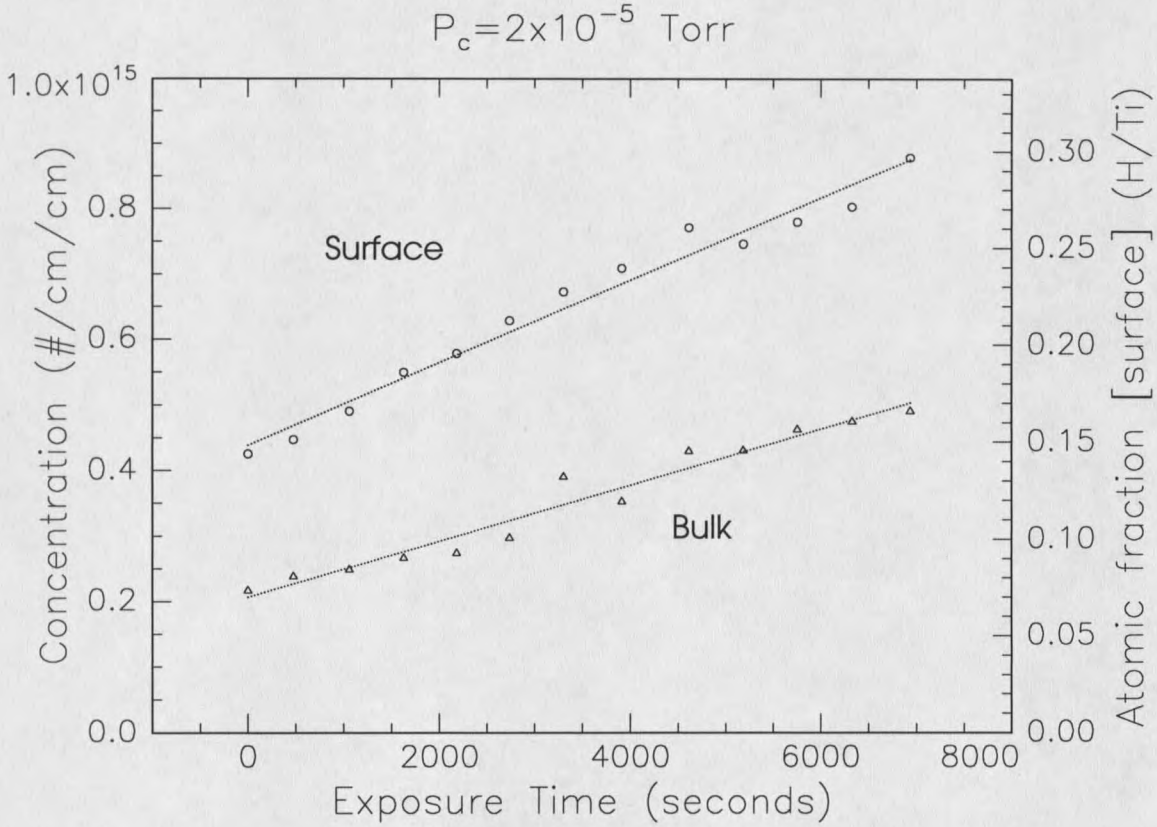

Figure 5.2.2

Hydrogen uptake in titanium.

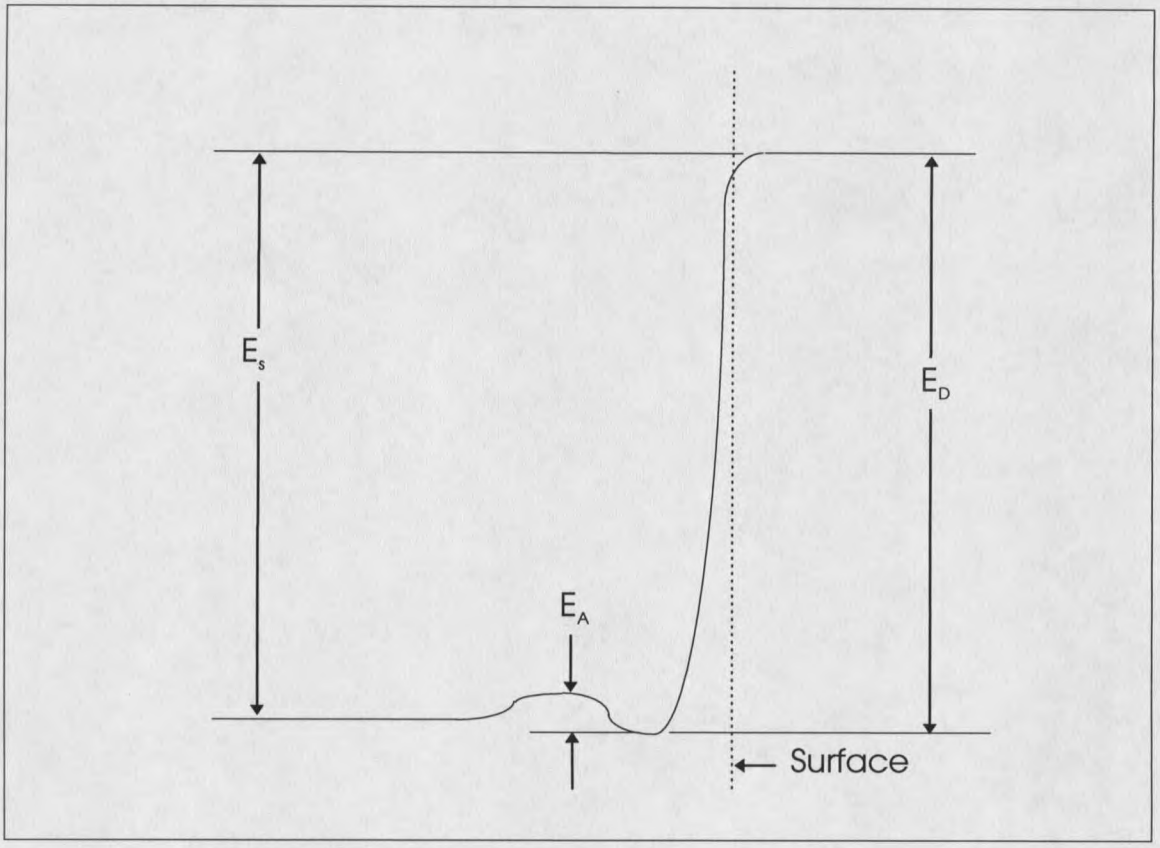

Figure 5.2.3

Exposure model's potential well for titanium based on computed barrier energy. The values for the energies are $E_S = 2.9eV$, and $E_D = 3.0eV$,[14] and the computed barrier energy is $E_A = 0.259eV$.

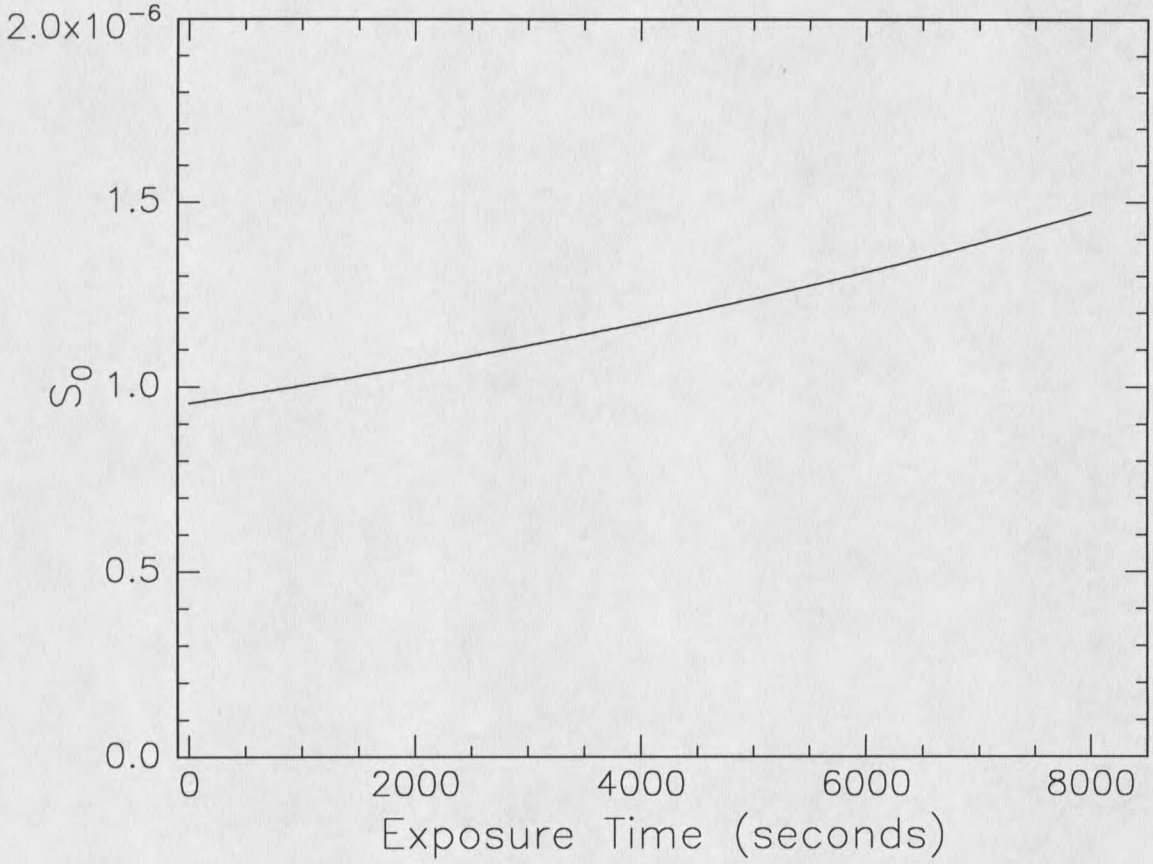

Figure 5.2.4

Sticking coefficient as a function of time.

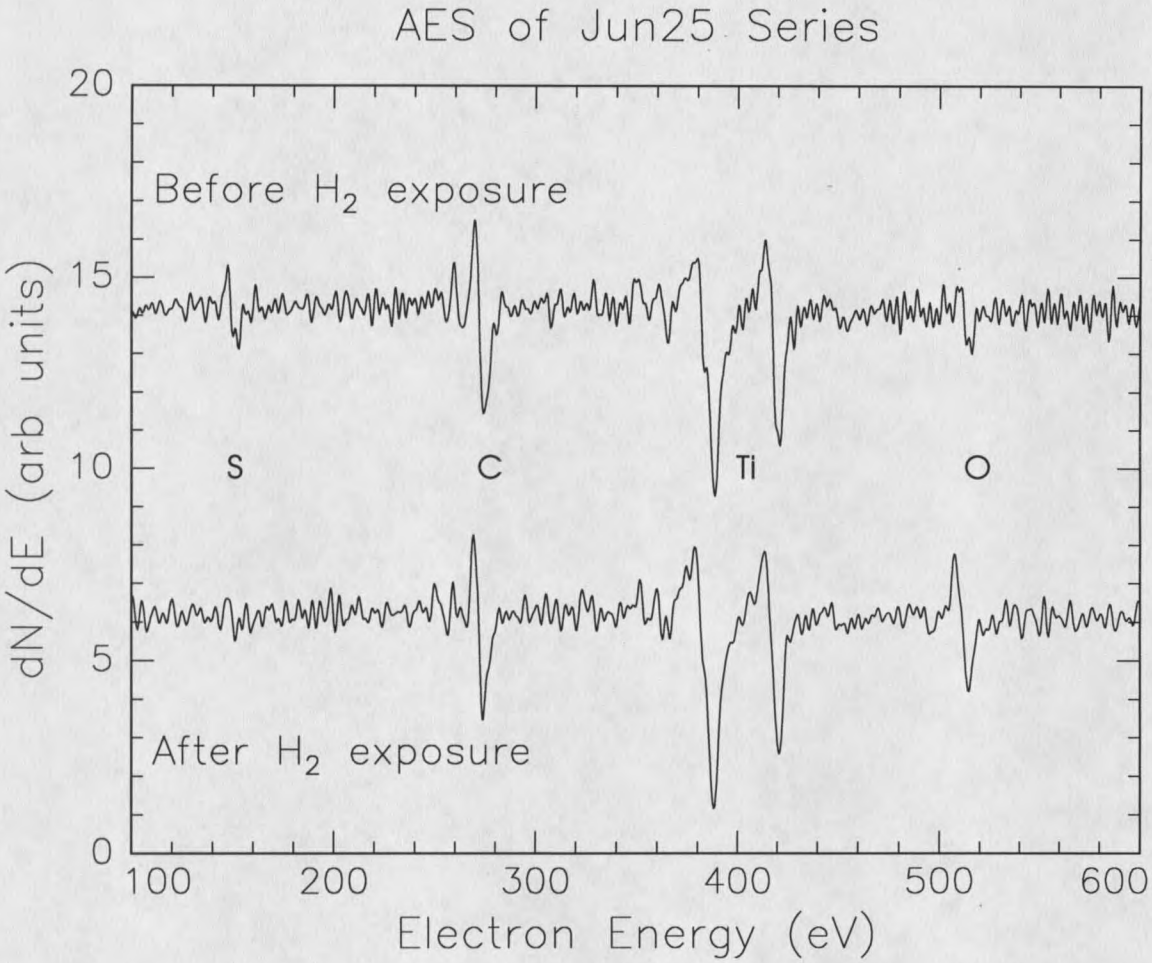

Figure 5.2.5

Surface characteristics of titanium surface for June 25th exposure series.

Note that the sulfur has been removed as a result of the exposure.

6. DISCUSSION AND CONCLUSIONS

The study of hydrogen absorption in titanium led to some interesting results. Despite the difficulties presented by straggling in the stopper foil, ERDA measurements allowed the determination of surface hydrogen distinctly different from the bulk hydrogen. Careful analysis of the ERDA spectra combined with the model of absorption, presented in section 4, revealed the process to include both surface and bulk properties of the hydrogen uptake. Furthermore, the functions used to fit the data showed that during the uptake process, surface hydrogen concentrations rose more rapidly than those of the bulk. It was also noted that hydrogen absorption depended upon the amount of surface contamination.

In a typical ERDA spectrum, the straggling due to the stopper foil had the effect of smearing the data. However, the spectra had a gaussian shaped peak near the surface while the rest of the spectra seemed relatively constant. The shape demanded that regions near the surface had higher concentrations, but the exact distribution near the surface was not known. The Davenport model[14] (section 4) had suggested that the surface hydrogen had position only in the first layer. If this was not the case, the width of the surface peak would not have been constant with respect to exposure.

Subsequently, the model represented an important step toward understanding the hydrogen uptake process. The internal energy barrier, E_A (see figure 4.1), controlled the rate of uptake by the bulk and the surface regions. Consequently, the best fits for the data

showed the existence of the barrier and determined that it remained constant. Though the nature of the barrier had not been determined, the value of approximately 0.26 eV suggested that surface strain of the crystal lattice had a contribution, since the computed value of the strain energy was 0.7eV. Thus, both strain and chemical bonds could contribute to the barrier energy.

Furthermore, the sticking coefficient for the process, S_0, having been variable throughout the experiments, was a potential difficulty with the model. The variable sticking coefficient suggested that the functions chosen for the fits were not the best choice. Regardless, the Davenport model had taken into account both surface and bulk properties of the hydrogen absorption process and had reasonably explained the experimental results.

The continuous exposure experiment was extremely sensitive to surface contaminants, as evidenced by the sulfur reduction in the continuous exposure experiment. Clearly, prior to attempting any modification to the functional fits, the effects of surface contamination upon the sticking coefficient has to be addressed. Furthermore, the sticking coefficient in the continuous exposure experiment was unexpectedly low; it seemed that the presence of the contaminants altered the process significantly, making sticking a very unlikely event. Some process, other than the Davenport model dominated the sticking event. A better model might define the sticking coefficient as a function of contaminant concentration:

$$S_0 = S_0(f_C, f_O, f_S, \ldots) \tag{6.1}$$

with f_x representing the fractional concentration of the contaminant. Regardless, future

experiments would require an increased attention to contaminant concentrations.

Ultimately, ERDA and the Davenport absorption model had been demonstrated as useful tools for understanding the hydrogen absorption process in titanium. Future experiments should expand on this work, should address the uptake properties of other metals that had been subjected to the Davenport model, and should indicate if the Davenport model is in error for saturation conditions present in the March 28th experimental series. Ultimately, ERDA was demonstrated to be an effective technique for determination of absorption characteristics of titanium and should be expanded to the studies of titanium based alloys intended for aerospace usage.

REFERENCES

1. H. G. Nelson, **Summary Proceedings of the 4th Workshop on Hydrogen-Material Interactions**, February 1993, p1.

2. M. Strongin, J. Colbert, G. J. Dienes, and D. O. Welch, Phys. Rev. B **26** (1982) 2715.

3. B. Kasemo, E. Törnqvist, and P. K. Johnasson, Chem. Phys. Lett. **68** (1979) 416.

4. R. H. Schaus and R. J. Smith, **Auger Electron Spectroscopy**, Montana State University (1992).

5. **Handbook of Auger Electron Spectroscopy**, Physical Electronics Industries.

6. J. R. Tesmer and M. Nastasi ed., **Handbook of Modern Ion Beam Materials Analysis**, (1995).

7. A. Turos and O. Meyer, Nucl. Inst. and Meth. **B4** (1984) p92.

8. W. K. Chu, J. W. Mayer, and M. A. Nicolet, **Backscattering Spectrometry** (1978).

9. F. Besenbacher, J. U. Anderson, and E. Bonderup, Nucl. Inst. and Meth. **B4** (1980) p1.

10. Adli A. Saleh, Phd. Thesis, Montana State University (1994).

11. J. E. E. Baglin, A. J. Kellock, M. A. Crocket, and A. H Shih, Nucl. Inst. and Meth. **B64** (1994) p469.

12. H. H. Anderson and J. F. Ziegler, **Hydrogen Stopping Powers and Ranges in All Elements** (1977).

13. J. F. Ziegler, **Helium Stopping Powers and Ranges in All Elements** (1977).

14. J. W. Davenport, G. J. Dienes, and R. A. Johnson, Phys. Rev. B **25** (1982) p2165.

15. W. E. Wallace, Q. Zhong, J. Genzer, R. J. Composto, and D. A. Bonnell, J. Mater. Res. **8** (1993) p1629.

16. B. Kasemo and E. Törnqvist, Appl. Surf. Sci. **3** (1979) p307.